

**Integrated Wide-band Mach-Zehnder
Interferometer for Wavelength Division
Multiplexing (WDM) Networks**



By:
ADEEL AKHTAR
2011-MS PhD-IT-025

Supervisor:
Dr. Usman Younis

Department of Computing
School of Electrical Engineering and Computer Science

National University of Science and Technology
Islamabad –Pakistan

2014

Integrated Wide-band Mach-Zehnder Interferometer for Wavelength Division Multiplexing (WDM) Networks



By

Adeel Akhtar

2011-NUST-MS PhD-IT-025

Supervisor

Dr. Usman Younis

This thesis is submitted in partial fulfilment of the requirements for the degree
of Master of Science in Information Technology MS (IT)

to

School of Electrical Engineering and Computer Science,

National University of Sciences and Technology (NUST),

Islamabad, Pakistan

October - 2014



NUST School of Electrical Engineering and Computer Sciences

A center of excellence for quality education and research

Certificate

Certified that the contents of thesis document titled “ Integrated Wide-band Mach-Zehnder Interferometer for Wavelength Division Multiplexing (WDM) Networks ” submitted by Mr. Adeel Akhtar have been found satisfactory for the requirement of degree.

Advisor: _____

(Name)

Dr. Usman Younis

DR. USMAN YOUNIS
ASSISTANT PROFESSOR
National University of Sciences
& Technology, Islamabad

Committee Member1: _____

(Name)

Dr. Salman Abdul Ghafoor

Committee Member2: _____

(Name)

Mr. Ahsan Azhar

Committee Member3: _____

(Name)

Mr. Yasir Iqbal

To My Maternal Uncle

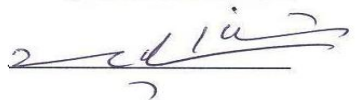
Mr. Shabbir Ali (Late)

CERTIFICATE OF ORIGINALITY

I hereby declare that the research paper titled “*Integrated Wide-band Mach-Zehnder Interferometer for Wavelength Division Multiplexing (WDM) networks*” is my own work and to the best of my knowledge. It contains no materials previously published or written by another person, nor material which to a substantial extent has been accepted for the award of any degree or diploma at SEECS or any other educational institute, except where due acknowledgment, is made in the thesis. Any contribution made to the research by others, with whom I have worked at SEECS or elsewhere, is explicitly acknowledged in the thesis.

I also declare that the intellectual content of this thesis is the product of my own work, except to the extent that assistance from others in the project’s design and conception or in style, presentation and linguistic is acknowledged. I also verified the originality of contents through plagiarism software.

Author Name: Adeel Akhtar

Signature: 

ACKNOWLEDGEMENT

I would like to express my gratitude to my supervisor Dr. Usman Younis for the useful comments, remarks and engagement through the learning process of this master's thesis. Besides, I wish to thank the participants in my research who have willingly shared their precious time during the process of questioning. Furthermore, I would remain thankful to Mr. Muhammad Zulqarnain (Campus Manager – Virtual University) who supported me to avail this master's opportunity. I would also like to thank my loved ones, who have supported me throughout the entire process, both by keeping me harmonious and helping me putting the pieces together. I will be thankful forever for your kindness & love.

Last but not least, I acknowledge the unconditional support of my parents, maternal uncle and fellows who continually support me during all the ups and downs of the way.

Table of Contents

List of figures	VIII
List of acronyms	X
Abstract	XII
Chapter 1. Introduction to Optical Switches	1
1.1 Introduction	1
1.2 Optical Transmission Systems	1
1.3 Multiplexing techniques in optical networks	2
1.4 Performance of a WDM network	5
1.5 Photonic Integrated Circuit (PIC) Switches	9
1.5.1 Mechanical Switches	9
1.5.2 Guided wave switching	9
1.6 Thesis contribution and scope	15
1.7 Thesis Organization	15
<i>Chapter Summary</i>	16
Chapter 2. Literature Review	17
2.1 Multimode Interference (MMI) Couplers	17
2.2 Mach-Zehnder Interferometers (MZIs)	19
2.3 Our device configurations	23
<i>Chapter Summary</i>	24
Chapter 3. Material Properties and Design	25
3.1 Material Design	25
3.2 Waveguide	26
3.3 Waveguide Design	27
<i>Chapter Summary</i>	29

Chapter 4.	Multimode Interference Coupler	30
4.1	Introduction	30
4.2	Self-Imaging and Multimode Interference	30
4.3	Multimode Interference Coupler design	34
	<i>Chapter Summary</i>	38
Chapter 5.	Mach-Zehnder Interferometer for optical switching	39
5.1	Introduction	39
5.2	Switch Design	40
5.3	Results and Discussions	44
5.4	Comparison with reference paper	48
	<i>Chapter Summary</i>	49
Chapter 6.	Conclusion & Future work	50
6.1	Thesis Summary	50
6.2	Future work	51
	References	52

List of Figures

Figure 1.1:	Two multiplexing methods to increase the capacity of transmission, (a) time division multiplexing and (b) wavelength division multiplexing. The modulated signal provides the time frames available for each logical state (0 or 1).	3
Figure 1.2:	(a) A packet switched network architecture and (b) a demonstration of WDM type network. A ring network is connected to the WDM stream network with the aid of a cross-connect. End users gain access to the network via add-drop multiplexer (ADM).	4
Figure 1.3	A Typical architecture of a three channels optical cross-connect (OXC).	6
Figure 1.4:	The most commonly used switch architectures. In structures (a), (b), (c) and (d), switching is obtained by refractive index change, architecture (e) is based on a semiconductor optical amplifier (SOA). The grey lines indicate the parts where refractive index is to be adjusted.	11
Figure 2.1:	Schematic diagram of 2×2 MMI coupler. Dark lines indicate the conventional structure while the optimized structure is represented with dotted lines.	18
Figure 2.2:	A 2×2 MMI coupler with tapered structure with having the length L and width $2w+h$ a) 2-D view b) 3-D view	18
Figure 2.3:	Schematic layout of MZI based switch using GeTe	21
Figure 2.4:	A 2×2 MZI structure proposed in [53].	22
Figure 2.5	Schematic structure of multimode interference coupler based optical switch . .	22
Figure 3.1:	Cross section of a) Shallow etched waveguide b) Deep etched waveguide. . .	27
Figure 3.2:	a) The constituted $2 \mu\text{m}$ wide and $3.2 \mu\text{m}$ deep etched waveguide structure and b) Contour map of TE_{00} mode of the designed deep etched waveguide. Dotted lines indicate the waveguide boundaries.	28
Figure 3.3:	Simulated effective index (n_{eff}) for the first three TE modes as a function of waveguide width	29
Figure 4.1:	Self-imaging properties of multi-mode waveguide.	34
Figure 4.2	Layout of a 2×2 MMI coupler (general interference regime)	35
Figure 4.3:	2×2 MMI coupler coupler with restricted paired interference regime	35

Figure 4.4:	A 3-D BPM simulation of general interference coupler having the physical width of 4.5 μm . It can be shown that the coupling length for 3 dB operation appears at 100 μm	36
Figure 4.5:	a) A 3-D simulation of 3 dB coupler, b) Transmission analysis of the designed 3dB coupler	37
Figure 5.1	Schematic structure of Mach-Zehnder Interferometer based optical switch . . .	40
Figure 5.2:	Graphical representation of a) cross state b) bar state	42
Figure 5.3:	a) Impact of current density on effective index of waveguide b) Effective rate of change with respect to the current density	43
Figure 5.4:	Output ports switching with respect to current intensity	44
Fig. 5.5:	Transmission window along with different tuning impacts a) cross state b) bar state	45
Figure 5.6:	Transmission of both switch states a) OFF state b) ON state	46
Figure 5.7:	Crosstalk on BAR when switch is on cross state	47
Figure 5.8:	Crosstalk on BAR when switch is on cross state	48
Figure 5.9:	The switching characteristics of the MZI switch with respect to the injected current	49

List of Acronyms

AlGaInAs	Aluminium Gallium Indium Arsenide
AMZI	asymmetric Mach-Zehnder interferometer
BPM	beam propagation method
OCDMA	Optical Code Division Multiple Access
DWDM	Dense Wavelength Division Multiplexing
EDFA	Erbium doped fibre amplifier
ER	extinction ratio
FP	Fabry-Perot
FSR	free spectral range
FWHM	full width half maximum
GaAs	Gallium Arsenide
GaInAsP	Gallium Indium Arsenic Phosphide
GRIN SCH	graded index separate confinement hetero-structure
InP	Indium Phosphide
MMI	Multi-mode interference
MQW	multiple quantum-well
MZI	Mach-Zehnder interferometer
OTDM	optical time division multiplexing
QCSE	quantum coned stark effect

QWI	quantum-well intermixing
RF	radio frequency
TM	transverse magnetic
TE	transverse electric
SOA	semiconductor optical amplifier
SONET	synchronous optical network
SDH	synchronous digital hierarchy
DC	Direct Current
WDM	Wavelength Division Multiplexing
ITU	International Telecommunication Union

ABSTRACT

Wavelength Division Multiplexing (WDM) is a very attractive option to satisfy the rapidly growing bandwidth needs. Multiplexing devices made it possible to exploit the real bandwidth of optical fibre. An optical switch is a key device while performing the reconfigurable multiplexing operations. Several number of wavelength switches have been demonstrated which are based on various approaches. Mach-Zehnder interferometer based structure is considered as efficient due to its characteristics, such as: low crosstalk, low insertion loss, and fabrication simplicity.

We have designed an optimal two channels tuneable wavelength switch based on Mach-Zehnder interferometer (MZI). The material used for the fabrication of the device is a compressive strained multiple quantum well (MQW) grown to a silicon doped InP wafer. We have analysed the waveguide and multimode interference (MMI) coupler to be used in our device. Two MMI couplers of $\sim 100 \mu\text{m}$ length and $4.5 \mu\text{m}$ of width have been used in our design due to their high bandwidth, low loss, and low crosstalk characteristics. A $400 \mu\text{m}$ long active phase-shifter is set in one of the two arms of MZI for the phase shift function as well as wavelength tuning. Wavelength tuning is obtained by injecting the DC biased current in the phase-shift region. The device analysis, on the basis of bandwidth and crosstalk, was performed by using Beam Propagation Method (BPM). A FWHM bandwidth of about 390 nm is achieved at the central wavelength 1550 nm . The transmission loss is recorded as low as 24 dB while a crosstalk of -38 dB has to be discovered in our solutions.

Chapter 1

Introduction to Optical Switches

1.1 Introduction

A rapidly growing number of **World Wide Web** users is increasing the bandwidth consumption due to the involvement of HD videos, images, interactive media and video-on-demand in data transfers. Traditional electrical domain technologies are, however, unable to fulfil these demands. So, there was a need of new technologies to be deployed. While investigating the various technologies, optical fibre seemed to be the most suitable among all due to its superior bandwidth capability and low loss. Different kind of multiplexing techniques i.e. Time Division Multiplexing (TDM) and Wavelength Division Multiplexing (WDM) have been introduced for the optimal use of available bandwidth. A closer look will be taken on these multiplexing techniques later, in this chapter. Further, the requirements, to be imposed on the components of optical network, would be investigated in later sections of this chapter.

1.2 Optical transmission systems

Optical networks were evolved since 1970's as an alternate data transfer system to the conventional electronic data networks. This could be done because of the LASER's invention [1] and glass fibres with a tolerable optical loss of 20 dB/km [2]. The optical frequencies, to be applied in these networks, such that a much larger bandwidth could be possible to achieve as compared to the available alternates; electronic data networks. This property of optical networks makes them very suitable to satisfy the ever-growing bandwidth demands.

In the last two decades, a large number of fibre optic links, having low losses and attenuation, have been deployed. In the start, these links were digital which were consisting the voice lines

of 34 Mb/s for trunking of telephone links. With the passage of time, more complex transmission techniques were realised to achieve the higher bit rate.

After that, the focus was moved to reduce the number of amplifiers and much expensive repeaters in the deployed optical networks. It was, then, realized that the optical signal attenuation must be reduced to reduce the number of network devices that increase the cost. After immense experiments, it was committed that the wavelengths around 1550 nm exhibits the lowest attenuation; as low as 0.15 dB/cm. Thus, the 1550 nm wavelength window is preferred on the conventional 1300 nm zero dispersion window. The availability of the Erbium Doped Fibre Amplifier (EDFA) which has the ability to amplify the optical signal between 1530 nm to 1560 nm is an added advantage of using the 1550 nm window. The wavelength window, supported by the EDFA, exhibits a bandwidth of about 4 THz. This implies that the theoretical bandwidth of a single optical wavelength, at 1550 nm, is 8 Tb/s [3]. Since the 1550 nm wavelength window is much wider than the EDFA window, thus its total theoretical transmission capacity is about 50 Tb/s before the losses to be incorporated [4].

At the day, the exploitation of real bandwidth of fibre optics is a challenging task because the devices, being used in optical networks like detectors and modulators, have bandwidths of smaller than 20 GHz. One possibility of using the available bandwidth, with the available devices, as much as possible is by using the multiplexing techniques.

1.3 Multiplexing techniques in optical networks

The simplest way to extend the transmission capacity is to install the additional fibre cables; space division multiplexing. Is it a practical approach? The answer in “NO” due to its high cost. So, the multiplexing techniques in optical networks were evolved to efficiently increase the transmission capacity of the network without installing the additional fibre. The first method is to combine several lower data streams to formulate a higher bit rate by employing higher speed electronics at the optical network terminals. This process is by means of Time Division Multiplexing (TDM) where time slots are divided into multiple sub-slots which are distributed to the end nodes. Each node (input channel) transmits its data only in time slot assigned to it. Fig. 1.1a illustrates this methodology where three low data streams are combined. The assignment of time slots is performed by a high speed multiplexer. At the other end, the routing of these data streams is performed by another de-multiplexer. The interleaving could be carried out on packets or bits basis. It becomes more and more difficult for switches

to handle the data as the data speed increased. The solution of this problem is routing of data through the optical domain which is named as Optical Time Division Multiplexing (OTDM). The single channel experimental speed of the OTDM systems is 100 Gb/s which is further reduced by the physical effects influence like chromatic dispersion and other non-linear elements.

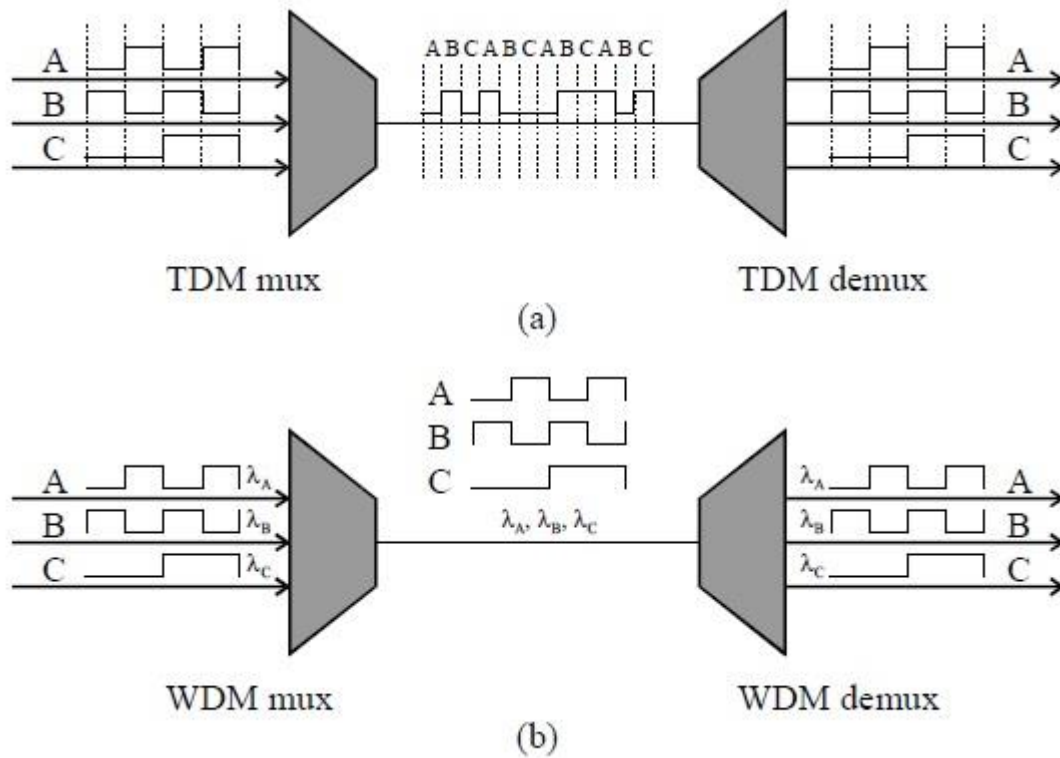


Figure 1.1: Two multiplexing methods to increase the capacity of transmission, (a) time division multiplexing and (b) wavelength division multiplexing. The modulated signal provides the time frames available for each logical state (0 or 1).

Apart from the high bit rate, obtained by the OTDM, still there is a huge unused bandwidth in the 1550 nm window which further needs to be exploited. A better use of bandwidth could be possible if together the additional wavelengths with the existing channel. This technique is called as Wavelength Division Multiplexing (WDM) where multiple wavelengths are combined and routed to a single mode fibre. Fig. 1.1b shows this methodology where three different wavelengths are being combined. The number of wavelengths in a WDM system is determined by the various factors like channel spacing and crosstalk level of the multiplexers (filters) employed in the network. Again, non-linearity's effects of the fibre are also considered while analysing the maximum number of channels.

A higher transmission capacity of a network can be achieved either by increasing the bit rate (OTDM) or by increasing the number of wavelengths (WDM). Due to the complimentary nature of both the techniques OTDM and WDM, it is also possible to combine both of them, which further increase the transmission capacity up to 3 Tb/s [5].

The simplest implementation of WDM and OTDM networks is the broadcast and select network where each node transmits in its own wavelength (in WDM) or in its own time slot (in OTDM). A central network device (multiplexer) combines all the signals and broadcast them to all the nodes which are connected to the multiplexer. After that, a selection of the desired signal is made by the each node. In more sophisticated OTDM network structures, a packet header is used (packet switching) to identify the appropriate stream. (Fig. 1.2a).

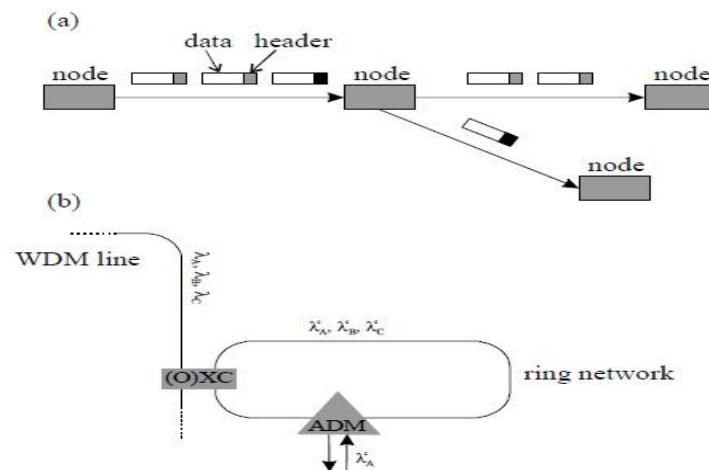


Figure 1.2 (a) A packet switched network architecture and (b) a demonstration of WDM type network. A ring network is connected to the WDM stream network with the aid of a cross-connect. End users gain access to the network via add-drop multiplexer (ADM).

The QoS, security and privacy are the common issues incorporated to the TDM networks. Such issues could be overcome in WDM networks with the implication of wavelength routing. Such nodes, in the network, are performed the routing which have the capability of shifting the stream of a specific input port to one of the various output ports. Add-Drop-Multiplexer (ADM) and optical cross-connects (OXCs) are used to perform the routing in WDM networks. ADM is used to add one or more new channels into existing stream or to remove one or more channels from the stream. OXC (switch) is used to transfer the data from one port to another. In Fig. 1.2b scenario, a cross-connect is responsible for shifting the streams from one ring to another ring.

The configuration of a simple reconfigurable cross-connect consist of (de)multiplexers and switches (Fig. 1.3). In a simple configuration, only an exchange of streams is possible. However, this simple configuration is no more worked where a wavelength λ_1 needs to be transferred from one network A to some other network B but in network B, λ_1 is already occupied. In such situation, wavelength converters need to be incorporated in cross-connect structure. A more sophisticated bandwidth utilization could be realized by assigning different wavelengths to a data stream. Further, other extra components like opto-electronic regenerators can be added to the cross-connect configuration according to the requirements. A special attention regarding to failure prevention is needed to design and establish a reliable network. In available failure prevention techniques, switches are being employed for traffic re-routing in case of failure occurred due to a fibre cut etc.

1.4 Performance of a WDM network

The physical layer of a high quality digital system determines the bandwidth requirements. The medium must be ensured the reliability of transmission from its source to destination [3]. This implies that the ration of successfully transmitted erroneous bits to the total number of transmitting bits should be minimum. This bit error rate is influenced by the various factors such as quality of the receiver with respect to the power per bit and noise level introduced by the network components. To date, the achieved Bit Error Rate (BER) is in the order of 10^{-15} to 10^{-9} . The available power in a network is highly dependent on the optical sources and amplifiers, glass fibre and attenuation introduced by the various network components.

The crosstalk in optical networks, introduced by the network components such as multiplexers and switches, is a very strong factor which influences the overall performance of a WDM network. It is a small portion of a wavelength power (optical signal) that ends up in a channel which belongs to another wavelength. The crosstalk, in WDM systems, can be of two types; intra-channel and inter-channel.

In case of intra-channel crosstalk, a crosstalk signal at the same wavelength is so close to the desired wavelength signal in such a way that the difference between both of the signals, crosstalk and desired, is within the range of receiver's bandwidth and hence, leaked into the desired signal. Usually, this type of crosstalk arises when a multiplexer and (de)multiplexer are cascaded. A part of the signal at some wavelength λ_1 leaks into the adjacent channels because of imperfect suppression in (de)multiplexer. When the multiplexer combines the wavelengths

to be transmitted on fibre, a small portion of crosstalk signal is, again, leaked back into the channel. Intra-channel crosstalk arises in this situation due to the delay in both the signals; crosstalk and desired one. When the multiplexers and (de)multiplexers are combined together with switches (fig. 1.3), an intra-channel crosstalk has to be observed at both output ports of the switch. This is because of imperfect suppression within the (de)multiplexer as well as due to mutual isolation imperfections of both switch ports.

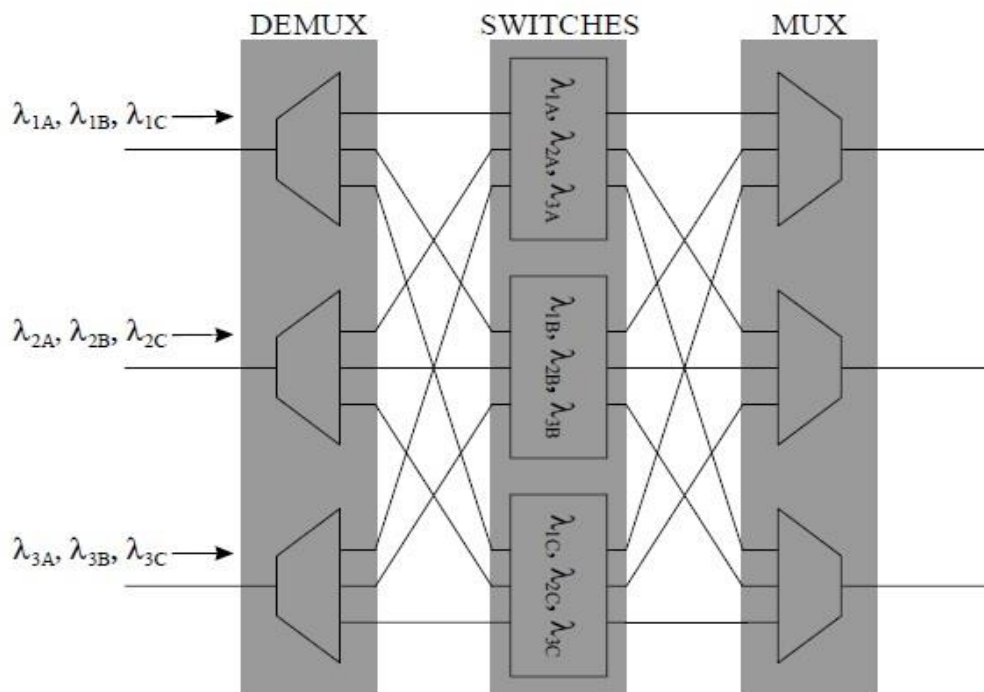


Figure 1.3 A Typical architecture of a three channels optical cross-connect (OXC)

In other case, inter-channel crosstalk, the crosstalk wavelength is sufficiently different from the wavelength of desired signal in such a way that the difference exceeds (generally) from the receiver's bandwidth. This results an incoherent addition of the power into the desired signal. The major factor of this kind of crosstalk is the use of such (de)multiplexers which select one channel while improperly reject the other channels. Using a 2x2 switch which is not properly isolating the output ports of the switch; also causes the inter-channel crosstalk. Along with the intra-channel crosstalk, the crosstalk signal also contains some part of the corresponding wavelength signal at the opposite port. Due to the coherence property of optical signal, an intra-channel crosstalk badly affects the bit error rate as compared to the inter-channel crosstalk. Thus, attention would be put on intra-channel crosstalk only when investigating the performance of the WDM system.

While designing the physical layer of the network, the crosstalk influence must be considered. Every crosstalk source that exhibits the undesired power to the undesired path, actually requires an increase in signal power at the receiver's end to maintain the required BER; a "power penalty". Knowing the power losses of the network and power penalties of each of the components causing the crosstalk, one can calculate the power budget of the whole network. Calculation of power budget is an important factor by which the requirements for the sources (lasers) and amplifiers could be determined and analysed.

The attenuation of a component can be increased by improving any specific property (e.g. crosstalk). This attenuation increase could be equal or larger than the power penalty; thus has no overall effect on the network performance or put a bad impact. Such methods, to reduce the crosstalk in switches, could be realized that emphasis on the overall switch loss. The relation between the obtained reduced crosstalk and the increased loss to an allowed limit indicates the improvement of network performance. This relation is analysed by calculating the power penalty as a function of crosstalk of a specific network element like a switch. This analysis is considered as a key of network configuration; the type of source and receiver as well as length of fibre along with the amplifiers.

Since, the complete network level analysis of all possible configurations is out of the scope of this thesis; so our investigation concern, in this thesis, will be about the power penalty due to the coherent crosstalk in the switch; which is definitely a few portion of overall network penalty.

Apart from the crosstalk requirements, the potential to meet the following requirements is also unavoidable.

- Polarization dependent loss
- Insertion loss
- Wavelength independence (in 1550 nm window)
- Response time
- Implementation simplicity (integration)
- Scalability
- Fabrication tolerance
- Reliability
- Power consumption

Since the single mode fibre could not maintain the polarization state thus the network components face the time varying and unknown polarization state. Because of this, the requirement of polarization independent operations has to be imposed.

The insertion loss should be minimized to ensure the network operations effective and efficient at various positions. Some network elements have different levels of losses for input-output signals. Thus, there may be required some additional devices (equalizers) to compensate these differences. Insertion loss could be due to different polarization states if the device, where the signal has to be inserted, has a polarization dependent behaviour and it puts a negative impact on the overall network performance. Therefore, it needs to be minimized as it can be.

Generally, in WDM systems, the applied wavelengths are of 1550 nm transmission window for low attenuation transmissions. So, it is a strong requirement that the network devices exhibit the wavelength independent behaviour within the said window to identically handle all the wavelength channels.

The response time of switches in optical network depends on the specific function of the switch. For example, in teleconferencing, telephony or other kind of long duration connections, a response time in milliseconds is allowed. Another dynamic property of switches is “protection switching”. It is about to re-route the optical signal to a secondary fibre in case of primary link failure. In such case the allowed response time could be much higher ranges from milliseconds to hundred milliseconds.

In usual, the optical components, fabricated in the form of Photonic Integrated Circuits (PICs), are much smaller than the electrical components [6] [7]. This behaviour of optical components simplifies the implementation and having a potential to integrate the various components onto a single chip unlike the electrical network components. However, the integration of components depends on the size of the circuit and the number of devices that can be integrated with PIC material. Scalability is an elementary property, while designing a switch, as it is supposed to perform a large number of input and output functions.

1.5 Photonic Integrated Circuit (PIC) switches

Till today, a number of PIC switches have existence which are distinguished by their material and geometry. The physical effect that is used for the switching purpose determines the geometry of the switch. The applications of a switch strongly depend on the particular properties of it i.e., response time and polarization dependence etc. The main types of switches are discussed in the following subsections.

1.5.1 Mechanical switches

These are kind of switches where the light manipulation is achieved by the displacement of waveguide/fibre or by the re-arrangement of the mirror on which the light beam is positioned to. The most promising device in this era is Micro Electro Mechanical System (MEMS) based switch [8] [9] where electrical actuators are used to rotate the mirror(s). This type of switches exhibits the low polarization dependence loss and very small level of crosstalk (less than -50 dB). The response time is considered as a disadvantage of mechanical switches (about 10 ms). Other disadvantages are inclusion of mechanical wears, vibrations sensitivity and their bad integration with other components in optical networks.

Experimental demonstration of these kind of switches with respect to response time in order of 1 minute and large switching structures of 512×512 have been demonstrated in [10]. MEMS switches are suitable for large switching structures due to their low losses but beam divergence and proper alignments are notable challenges on the other hand.

1.5.2 Guided wave switching

The switching requirement of a guided wave switch is on-chip routing. A number of structures have been proposed for this purpose. In following subsections, the geometries of these kind of switches are described. In most of this type of switches, a change in refractive index of the material is introduced to obtain the switching operations.

a) Geometries of space switches

In the recent past, a number of integrated optical switch architectures were proposed. Few of these architectures are designed for specific applications while others have their applications in more general. In this section the fundamentals of generally applicable switches will be discussed.

The Mach-Zehnder Interferometer based switch consists of two couplers which are connected by two interferometer arms. First coupler acts as a splitter which splits the input beam into two equal parts while the second coupler is used for combining two signals (constructive interference). The phase difference is achieved, by changing the refractive index of one of the arms, in such a way that the light switches from one port to another. The main characteristic of this type of switch is that the mode coupling part is separated from the phase shifting part such that the optimization of both the parts are independent of each other. Usually the required change in refractive index, for switching purposes, is sufficiently small which is normally achieved by current injection in one of the MZI arms or by heating effects. The setbacks of this type of switch are the length of fabricated device and accuracy in refractive index change is required for output port switching. A polarization insensitive and fabrication tolerant structure could be achieved when Multi-Mode Interference (MMI) couplers are employed for 3-dB operations.

In directional coupler switch, two waveguides are placed adjacently in such a way that the light can be transferred by coupling from one waveguide to another. In this type of switch, the switching is achieved by adjustment of refractive index in one of these waveguides. Like MZI based switch, the required change in refractive index is much smaller however an accurate coupling length is required for obtaining the best transfer of light. Since this waveguide length is wavelength and polarization dependant and is influenced strongly by fabrication deviations like waveguide spacing and etch depth so it is hard to achieve a good switching performance.

A waveguide crossing is involved in the total **internal reflection switch** to control the refractive index. Just like as MZI based switch, the switching of light from one output port to the other is achieved by changing the refractive index in such a way that the input light is transmitted or reflected by the cross section (Fig. 1.4c). A wavelength and polarization independent switching could be achieved with the sates of “zero bias” and “above the switching voltage” respectively. Generally, a higher effective index change is required for switching purposes which is obtained by current injection. This switching requirement is considered as the disadvantage of this type of switches because of the low switching speed and heating effects. Another notable disadvantage of total internal reflection switch is the requirement of high fabrication precision for the angle between waveguides.

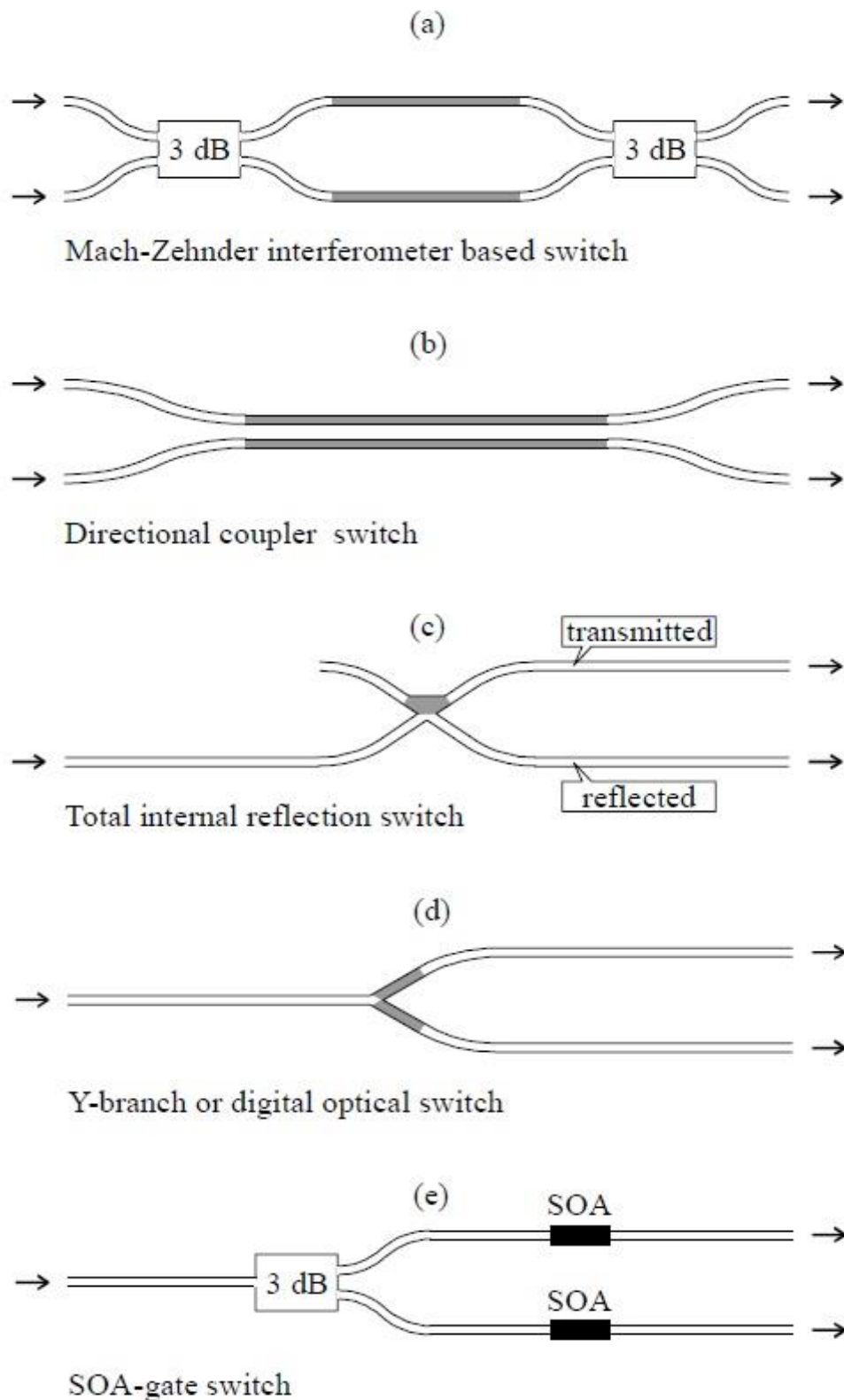


Figure 1.4: The most commonly used switch architectures. In structures (a), (b), (c) and (d), switching is obtained by refractive index change, architecture (e) is based on a semiconductor optical amplifier (SOA). The grey lines indicate the parts where the refractive index is to be adjusted.

The **Y-branch** switch uses an adiabatic mode evolution to switch the output ports. Again, switching is obtained by changing the effective refractive index in one of the two branches. The required refractive index change for switching purpose is higher than the MZI based switch which is achieved by the current injection or reverse bias. The digital response of the Y - branch switch is wavelength and polarization independent. The requirement of higher refractive index change for switching and accuracy for the fabrication of waveguide angles are the notable setbacks of these kind of switches.

b) Electro-optical switches

The carrier induced and electric field induced are the two classes of the physical effects by which electro-optical refractive index change could be obtained. The refractive index change by carrier induced is to be obtained by changing the carrier concentration. This could be done by plasma effects, band-gap shrinkage and band filing. The change in carrier concentration is achieved by depletion or by carrier injection. The major drawback of carrier induction is it has a long carrier recombination time which relatively slows down the speed as compared to the carrier depletion. For InP/InGaAsP based switches which function on carrier depletion, a switching speed of more than 1 GHz has been observed [11]. Further, a switching speed of about 10 GHz for this type of switches is observed when calculating the RC-time [12]. Linear and quadratic electro-optic effects are always accompanied to the carrier depletion effects. This is because of the presence of electric field in the depletion region. During the process of layer stack designing, a special attention is needed onto the layers thickness to ensure the minimum optical loss.

The change in refractive index by the electric field is because of quadratic (Kerr/Franz-Keldish) and linear (Pockels) electro-optic effects. Both InP/InGaAsP and lithium niobate [13] are suitable for the fabrication of switches which are based on electro-optic effects. The change in refractive index in both of the materials is almost same. An additional advantage of the InP/InGaAsP based switch is that amplifiers and detectors can be fabricated in this material. A notable disadvantage of the quadratic and linear electro-optic effects of zinc-doped semiconductors is the polarization dependence. This polarization dependence can be possible to remove in InP/InGaAsP material. This could be done by proper orientation of crystallographic axes of waveguide. Both of the Kerr and Pockels effects have a refractive index change response time from 10^{-14} to 10^{-13} seconds, by which a 100GHz of switching speed

is obtained [14]. For the traveling-wave electrodes switches fabricated with the materials lithium niobate or InP/InGaAsP, a switching speed of more than 10 GHz is measured [15][16].

The double hetero structure InP/InGaAsP layers stack is replaced with InP/InGaAsP multiple quantum well (MQW) or InGaAlAs/InAlAs multi-quantum well to strengthen the refractive index change by electro-optic induction. Thus, the change in refractive index by electric field is introduced which uses the quantum confined Stark effect (QCSE) [17]. In most cases, this effect is polarization dependent which is further possible to be removed with the aid of strain in electric InP/InGaAsP – MQW [18][19]. The main disadvantages of Stark effects are wavelength dependence and complications in technology for the growth of layers. Practically, the best obtained switching time for the QCSE employed switch is less than 70 ps [20], which allows a switching speed of more than 10 GHz.

The crosstalk level of electro-optic switch is determined by the switch type. The best achieved level of crosstalk in InP/InGaAsP material is less than -25 dB with a power penalty of about 2 dB [21] [22]. InP/InGaAsP - MQW based optical switches have a reverse biased operation which make them competitively suitable where high speed switching is required. On the other hand, the achieved crosstalk for this type of switches is -19 dB [23]. The reported crosstalk level for the MZI based switch is about -20 dB with a power loss of 2 dB [14]. MZI switches based on a MQW structure have slightly higher power loss of about 3 dB [24]. Electro-optical switches based on directional couplers are polarisation dependent. The optimal crosstalk level for the directional couplers based switches fabricated with the material InGaAlAs/InAlAs - MQW is -20 dB [20]. For the lithium niobate material, the observed crosstalk is between -15 dB and -30 dB [25]. The reported crosstalk and power loss for the MZI based switches fabricated with lithium niobate are -20 dB and 5 dB respectively [26]. The crosstalk level of a digital optical switch fabricated with the material lithium niobate is about -15 dB along with a power penalty of less than 2 dB [27]. Renaud has presented the detailed review about semiconductor optical space switch in [28].

c) **Thermo-optical switching**

The simplest approach to change the refractive index of a material is to change the temperature. This change of temperature is introduced by the heaters locally. This kind of switching is called as “*Thermo-optical switching*”. The switches under this category have been fabricated on polymer [29] [30] and silicon/silica materials [31]. The crosstalk level of less than -30 dB is

achieved for these materials. The drawback of these kind of switches is longer switching time (~1 ms). Other notable disadvantages are the device size which is comparatively large due to the smaller contrast of refractive index, thermal crosstalk and power consumption by the heaters.

d) Acousto-optical switching

Another way to change the refractive index, which is required for output port switching, of any material is to strain the material. Lithium niobate based switches have been fabricated by employing the “straining” principle. In these switches, the strain is realised by means of an acoustic wave propagation that enables wavelength selective switches to be realised. These switches are suitable for WDM networks as optical cross-connects and optical add-drop multiplexers (OADMs). The achieved crosstalk for these kind of switches is about -15 dB with a switching speed of 1 μ s [32] [33].

e) All-optical switching

Another technique to change the refractive index for switching is to introduce the semiconductor optical amplifiers (SOAs) in one or both arms of switch. This method is realised in InP/InGaAsP – MQW material. In this methodology, the carriers in SOA deplete by applying an optical control pulse to the SOA such that the refractive index and the gain is changed.

Unlike other type of switches, the electrical control is replaced by the optical control. The switches based on this principle exhibits the switching speed of 6 ps [34]. The experimentally achieved crosstalk for these switches is less than -20 dB [35]. The observed disadvantages of this category devices are the requirement of high power for the control signal, the small power range of the switches and the complications in fabrication techniques. Further, a deterioration in performance is observed when these circuits are integrated in a system with other components. This performance deterioration is because of the heat, produced in the SOAs.

f) Semiconductor Optical Amplifier (SOA) switches

A SOA can either be used for attenuation or amplification of optical signal by turn the “gain” ON or OFF. This property of SOA can be used effectively for switching the light beam. A 3dB splitter is employed to split the input signal power and pass through the two different arms where the signal is amplified in one arm and attenuated in other (Fig. 1.4e). This type of switch

has low losses as SOA compensates the losses and even gain. The major disadvantage of SOA based switch is that the noise level, produced in the ON state of SOA, is too high because of spontaneous emission in the SOA.

1.5 Thesis Contribution and Scope

This thesis serves to carry out the design and analysis of a 2×2 Mach-Zehnder Interferometer (MZI) based optical switch to be used in optical networks. An initial waveguide analysis is carried out followed by the multimode interference (MMI) coupler design and Mach-Zehnder Interferometer formation. The core simulations were performed in “RSoft BeamProp” to analyse the circuit performance. The effects of DC biased current on the waveguide refractive index are also studied in this thesis that are used for wavelength tuning and output port switching. The results of our designed device are compared with some existing devices of same cadre in literature.

Mach-Zehnder Interferometer based optical switch, designed in this thesis, would be used in optical networks to selectively switch the output fibre in case of cable cut; *resilience*. The other use of this circuit is in reconfigurable wavelength multiplexing devices (multiplexers) where a number of input wavelengths are combined to be transmitted to a single fibre (usually single mode). The device may not be performed well in multiplexing scenarios where time synchronization between all system nodes is a major concern by means of multiplexing; *synchronous time-division multiplexing*.

1.6 Thesis Organization

The thesis is organized in following units:

Chapter 2: The literature with respect to the Mach-Zehnder Interferometer based circuits is reviewed in this chapter.

Chapter 3: In initial sections of chapter 3, the material used for the fabrication of our circuit is discussed while the later sections discuss the initial waveguide design and analysis.

Chapter 4: The design of multimode interference (MMI) coupler with detailed analysis is presented in this chapter.

Chapter 5: Formation of Mach-Zehnder Interferometer (MZI) based optical switch and its performance analysis is carried out in chapter 5. The chapter discussions include the simulation results and comparison with circuits in literature to verify our thesis work.

Chapter 6: This chapter concludes the thesis along with the proposal for future work which may be planned in the same area of study.

Chapter Summary

An introduction to optical switches is presented in this chapter. The geometries of different type of switches along with the core performance metrics of these switches are discussed in great details. It is observed that the MZI based switches offer the higher bandwidth capacity as compared to others. Further, the transmission losses and crosstalk of these kinds of circuits are also lower. The later sections of the chapter describe the research contribution and thesis organization. The upcoming chapter is related to the literature review regarding to the Mach-Zehnder Interferometer based circuits.

Chapter 2

Literature Review

In this part of thesis, the highlights of Mach-Zehnder Interferometer (MZI) based circuits from the literature are presented. The configurations of these proposed devices along with their performance metrics are reviewed.

2.1 MMI Couplers

Multimode Interference (MMI) couplers are one of the key elements in optical networks that has significant contribution in the history of integrated circuits revolution. A list of proposals regarding to the MMI couplers do exist in literature with different configurations. Some highlights from the literature are being presented in following.

The 3-dB MMI couplers with the lengths from 15 μm to 50 μm have been proposed in [55]. The couplers have a strong lateral confinement because of using the tapered access waveguides deep dry etching. The sizes of proposed devices was significantly reduced by using the large S-bends. The noted excess losses for these circuits are comparatively higher than the others. When using as splitter, the devices show the imbalance of less than ± 0.5 dB.

The dispersion analysis of tapered and straight $N \times N$ MMI couplers is carried out in [60]. In this proposal the bandwidth analysis of SOI based MMI couplers is also presented. The authors claim that the bandwidth is reduced by increasing the channel number with channel guides center space. However, the crosstalk is reduced by increasing the guide space. An increase in guide space and channel number cause the increase in length and width of MMI region that reduces the signal bandwidth. As compared to the traditional straight MMI coupler, the bandwidth can be improved by using the tapered MMI coupler. It could be possible due to the mode mixing in tapered region and the length reduction.

An efficient design of MMI coupler is proposed in [61] to reduce the back reflections. It was shown that the back reflections are 10 dB less as compared to the conventional MMI coupler; *figure 2.1*. The optimization of Si nanowire waveguides MMI coupler is proposed in [62] for

polarization insensitive operations. The same beat lengths are obtained for both TE and TM polarization states by fixing the core height. The authors claim the 0.5 dB bandwidth of more than 60 nm is to be achieved for both polarizations. This design is suitable for $N \times N$ ports where N is less than 10.

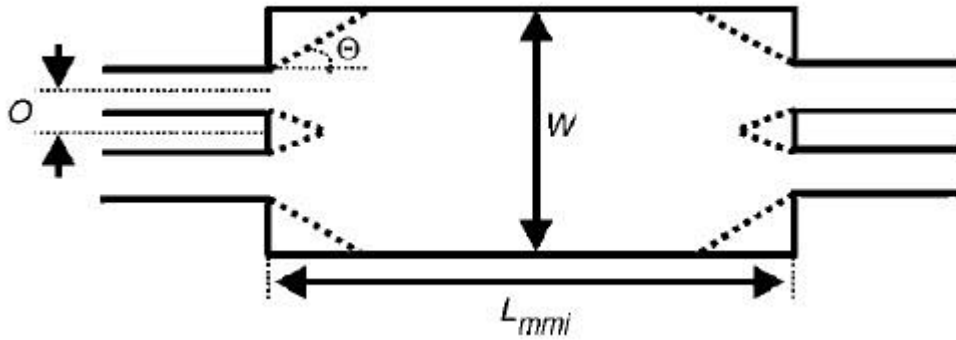


Figure 2.1: Schematic diagram of 2×2 MMI coupler. Dark lines indicate the conventional structure while the optimized structure is represented with dotted lines. [62]

Another MMI coupler with tapered structure is realized in [63]. The material used for fabrication of the device is $\text{SiO}_2\text{-SiON}$. The beat length of this proposed coupler is reduced by 45% as compared to the conventional structures. (Figure 2.2)

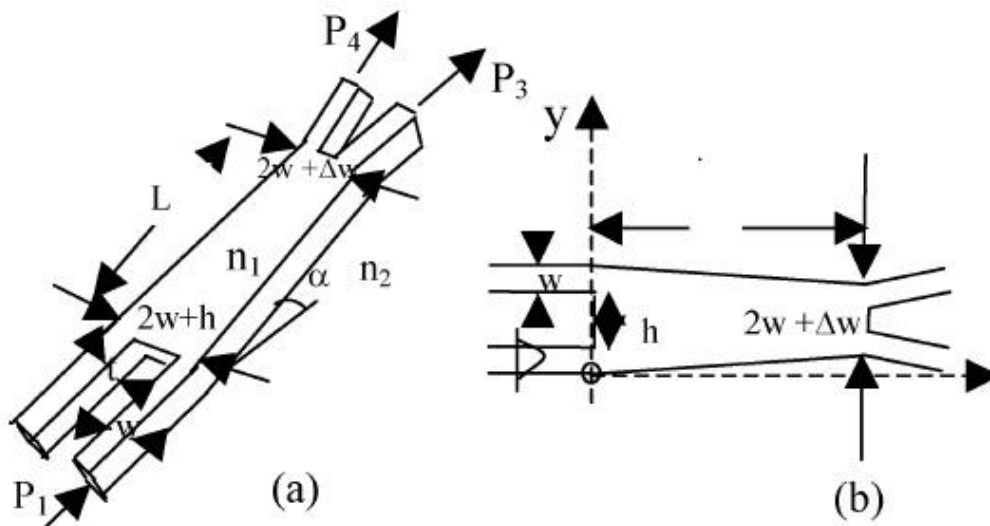


Figure 2.2: A 2×2 MMI coupler with tapered structure with having the length L and width $2w+h$ a) 2-D view b) 3-D view [63]

A wideband polarization coupler is presented in [64] that utilized the wavelength independent imaging effect and electro-optic effect for polarization splitting. The design problem is addresses by using the gradient based algorithm. This algorithm enables a user to efficiently

obtain the optimal design within few iterations. To provide the better performance in MZI structures, an MMI structure of compact size is investigated in [65]. The presented results in this article indicates that the MMI loss is reduced to the below 1 dB by widening the input and output ports to a width of 1 μm when to be used in MZI.

In [66], analytical formulae are proposed to design MMI couplers by using the general strip waveguide structure. The authors claim that these formulae are used effectively to optimize the MMI coupler design. Polarization in-sensitive device is achieved by fixing the core width in waveguide. This core width could be analyzed through the proposed analytical model.

2.2 Mach Zehnder Interferometer(s) (MZIs)

A number of Mach-Zehnder Interferometer based structures for wavelength switching, multiplexing, add drop multiplexing, modulating and demodulating has been proposed in literature. The configuration of the device highly depends on the application of the circuit. Since the scope of this thesis is limited to the optical switching applications so the optical switching highlights from the literature are presented in this section.

H.Y. Wong proposed a 2×2 tuneable optical switch in [44]. A multiple quantum well (MQW) structure of the material InGaAs–InAlGaAs is used to fabricate the device. The interferometer is formulated by combining two multimode interference (MMI) couplers of the dimensions of $6 \times 220 \mu\text{m}$. The proposed device is to be functional on the central wavelength 1550 nm. The authors, in this publication, claimed an experimental bandwidth of about 120 nm (1460 – 1580 nm) incorporated to their proposed switch. The device has the 400 μm long MZI arms on which active phase shifters are to be placed. The first cross to bar switching is achieved with a current injection of about 3.5 mA. The reported propagation loss of the proposed device is 19 dB and the crosstalk level is as low as -20 dB.

In [49], A Mach-Zehnder Interferometer (MZI) family device, composed of InAlGaAs/InAlAs/InP structure, is proposed for switching operations. It is a 2×2 optical switch that uses the active phase shifter in one of its arm for wavelength tuning. The tuning is obtained by injecting the current in this phase shifter. The switching is performed with the current density of 3.5 mA. The reported crosstalk level for this switch is as low as -20 dB for off state and -20.7 dB for ON state.

A 2×2 optical switch based on Mach-Zehnder Interferometer (MZI) is reported in [50]. The switch consist of two 3-dB directional couplers which are connected together by two arms of the same length. To formulate the symmetric MZI structure, thin films of GeTe are placed in both of MZI arms. These GeTe films are 20 nm thick and as wide as the silicon waveguide is (*figure 2.3*). The reported insertion loss of this device with respect to *cross* and *bar* are 0.5 dB & 3.45 dB respectively. The crosstalk level is -34 dB and -10.3 dB with respect to the *cross* and *bar* respectively. The claimed operational bandwidth for this circuit is about 80 nm.

Another 2×2 GaAs-GaAlAs carrier injection MZI family switch is presented in [51]. The MZI circuit is constituted with a couple of multimode interference (MMI) couplers having the dimensions of $20 \times 1983 \mu\text{m}$. A couple of 500 μm long electrodes is placed in two arms of MZI to change the waveguide refractive index. The total length of the circuit is about 1.4 cm. The results exhibit that the first cross to bar switching is occurred at the 15.8 mA of current injection in electrodes while the next bar to cross switching requires a 44.3 mA of current. The on-off extinction ration for this device is 21.5 dB and 20.6 dB for both the bar and cross states respectively. The measured insertion loss is about 2 dB and propagation loss is around 0.5 dB/cm for the 1550 nm wavelength.

In [52], the thermo-optic effects on a silica family Mach-Zehnder Interleaver are analyzed. Two 3-dB directional couplers are used in the proposed design of interleaver. The spectral response of the proposed circuit is periodic. These spectral periodicities are named as Free Spectral Range (FSR). The simulation results indicate the FSR of 8.2 nm while the channel isolation power is observed to be less than -50 dB. The obtained wavelength shift is 1.08 nm, 2.15 nm and 3.23 nm for the temperatures of 127⁰C, 227⁰C and 327⁰C respectively. Further, in the same article, a two stage cascaded Mach-Zehnder Interferometer is also analyzed that exhibits a crosstalk of -30 dB. According to the study, the single interferometer and the two stage cascaded design accept the same impact of thermo-optic effects.

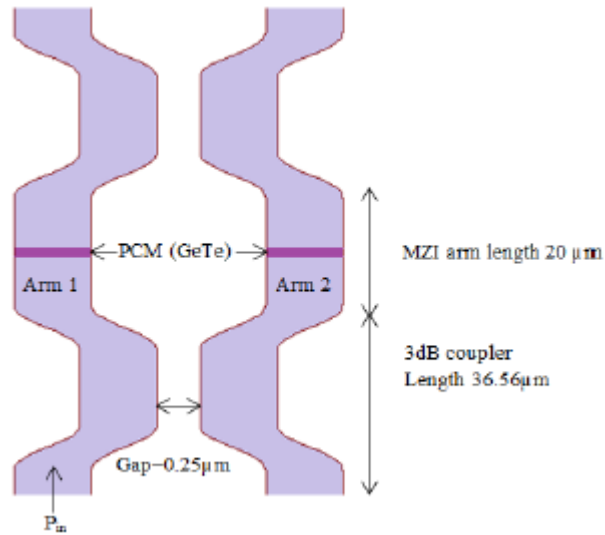


Figure 2.3: Schematic layout of MZI based switch using GeTe [50]

H. Y. Wong, W.K. Tan and A.C. Bryce were proposed a MZI family tunable wavelength demultiplexer in [53]. The presented circuit is a 2×2 asymmetric MZI circuit integrated by using the sputtered SiO_2 QWI process. It consists of two MMI couplers and phase shifters in each of the two arms of Mach-Zehnder Interferometer. These phase shifters are the active regions of the device which are used to tune the wavelengths on output ports of the MZI by injecting the current. The channel spacing of 0.8 nm was observed in results with an injection current of 6mA under the single arm operation. The initial extinction ratio of about 23 dB was noted which was further improved to 27 dB by reducing the imbalance of the power in the arms. The observed fiber-to-fiber loss is about 19 dB. Estimated on-chip losses are about 9 dB and 6 dB with no dc pre-biasing and dc pre-biasing respectively.

A multimode interference (MMI) coupler based optical switch is presented in [54]. The proposed circuit is essentially a multimode interference coupler (*figure 2.5*) where a heater is placed on one side of the coupler. The polymeric material is supposed to the fabrication of this device while the heater is placed on the polymeric films. The switching is obtained by the thermo-optic (TO) effect. The recorded crosstalk for the proposed switch is about -20 dB on both bar and cross ports while the incorporated power loss is less than 0.56 dB. The authors presented a 1×2 optical switch with the configuration of single heater on one side of MMI coupler. However, they claimed that the 2×2 switch with the same structure is obtained by placing another heater on the remaining side of the coupler.

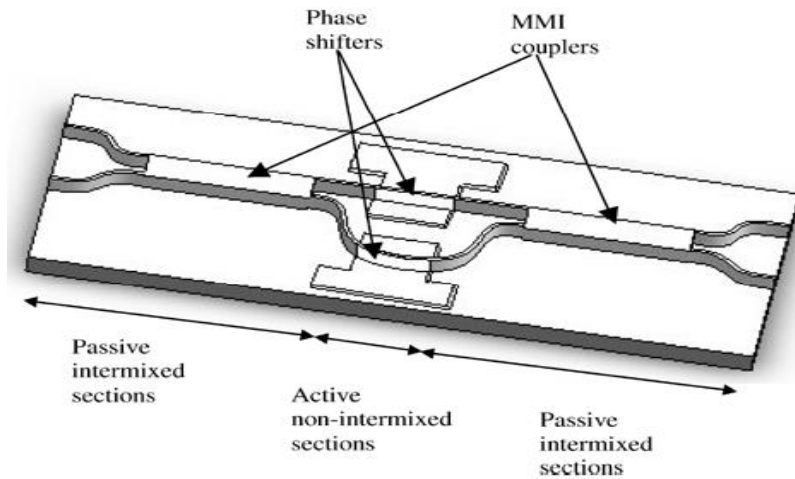


Figure 2.4: A 2×2 MZI structure proposed in [53]

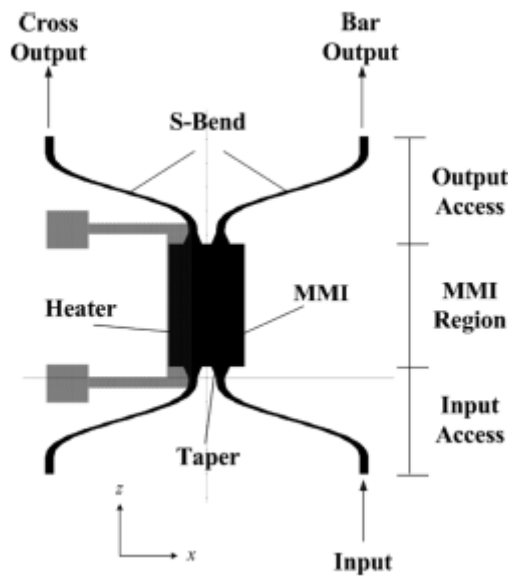


Figure 2.5 Schematic structure of multimode interference coupler based optical switch

The operation principles of optical switches that are based on two multimode interference (MMI) couplers are analyzed in [56]. The analysis of an 8×8 switch is carried out by using the analytical transfer matrix theory which is further verified through numerical simulations. The reported crosstalk for this circuit is about -22 dB.

Another study about the multimode interference coupler based optical switching is carried out in [57]. Despite to the self-imaging properties of the multimode interference coupler, the proposed approach focuses on the length of coupler. According to the proposal the coupler's

length should be smaller than the length of first self-image. The switching is obtained by launching another input field in the input port other than that where the original input signal is launched. By injecting the extra input field along with the original input signal, the interference occurs in multimode region which makes the switching possible. Thus, the proposed switch can be introduced in terms of two insertion fields. The reported insertion loss and crosstalk are 0.12 dB and -28 dB respectively with respect to the bar port. An insertion loss and the crosstalk of about 0.13 dB and -31 dB are observed respectively when the switching is performed from the bar to cross.

2.3 Our device Configurations

A number of configurations to formulate the MZI has been proposed in literature. Some authors, who have built their interest towards the reduction of losses that occurred due to back-reflections and tunability characteristics of the couplers, have used “*directional couplers*” to constitute the switching circuits. In few configurations, the authors gave preference to “*Y-junction couplers*” due to their no polarization sensitivity and very short size. Another group of authors has used MMI couplers in their circuits due to low crosstalk and good fabrication tolerance characteristics of MMI couplers. All these configurations have their own pros and cons.

The performance metrics to whom we concerned, in this study, are propagation losses, crosstalk and bandwidth. In order to formulate a MZI circuit while achieving the higher performance with respect to the mentioned metrics, we used MMI couplers in our design as they are proved for higher bandwidth support, compact device size, good fabrication tolerance, low crosstalk and negligible polarization sensitivity. In our design, a couple of 4.5 μm wide and 100 μm long MMI couplers are used to constitute the MZI switch. These couplers are connected through a couple of 2 μm wide and 400 μm long waveguides; so called arms. In one of these arms, an active phase shifter is placed for wavelength tuning and phase shift purpose. This is the actual portion of the circuit which is responsible for switching between the output ports.

Other configurations which use the “*directional couplers*” can be used to achieve the same goal for which our proposed device has to be constituted. But these configurations lead to the lower number of wavelengths to be supported and the resultant device is sensitive to polarization and has a higher level of crosstalk. For the cases of “*Y-junction couplers*” based configurations, the

obtained bandwidth is again significantly low as compared to our configurations and device exhibits the high back-reflections.

Chapter Summary

The different configurations, from the literature, to formulate the MZI circuit are reviewed in this chapter. The pros and cons of each configuration has been analyzed theoretically in order to establish the MZI based optimal switch according to our concerned performance metrics; crosstalk, bandwidth and transmission losses. At the end of chapter, the MZI configuration that is used in this thesis is elaborated. In our thesis, we configured the MZI switch by using the MMI 3 dB couplers and wavelength tuning is obtained by injecting the DC biased current in one of the two MZI arms. In next chapter, a brief discussion about the material that is used to fabricate our proposed switch is carried out along with the initial waveguide design and analysis.

Chapter 3

Material Properties & Waveguide Design

The material used for the fabrication of waveguides is discussed in this chapter. First, a brief overview of material properties is given then the basic waveguide structure, which is further used to design the other components in subsequent chapters, is discussed in later sections of this chapter.

3.1 Material Design

The invention of quantum well intermixing lead the waveguide theory to be entered into a new era. It enables the passive regions to be integrated at the facets of laser diodes that offers the excellent performance and increase the reliability of optical systems. The quantum well is a potential well which has only discrete values of energy. A quantum-well is based on a thin layer which is formulated by semiconductor material. This layer is sandwiched between two wider band-gap material layers wherein transpiration of quantum effects occurs.

A commercially available multiple quantum well (MQW) structure is used for the fabrication of all the components in this thesis. The layers structure of the wafer design is shown in *table 2.1* [39]. Five quantum well layers are used which are sandwiched between the two 60 nm thick graded index layers. These graded index (GRIN) layers are to ensure the better optical confinement. All these layers are further sandwiched in the two wide band-gap layers to prevent the holes and electrons to be escaped from the quantum well. In the experimental studies, it is observed that the conduction band offset of AlGaInAs/InP is larger as compared to the InGaAsP/InP materials. Thus, the Al-quaternary materials based devices have a high temperature characteristics and low carrier leakage [36]-[38].

<i>Thickness</i>	<i>Material</i>	<i>Layer</i>	<i>Dopant</i>	<i>Ref. Index</i>
200 nm	Ga _{0.47} In _{0.53} As	Cap	Zinc	3.646
50 nm	Ga _{0.29} In _{0.71} As _{0.62} P _{0.38}	Lattice match	Zinc	3.470
1600 nm	InP	Upper cladding	Zinc	3.146
20 nm	Ga _{0.15} In _{0.85} As _{0.33} P _{0.67}	Wet etch stop	Zinc	3.310
50 nm	InP	Transition Layer	Zinc	3.146
60 nm	Al _{0.42} Ga _{0.05} In _{0.53} As	Electron confinement	Zinc	3.279
60 nm	Al _{0.34} Ga _{0.13} In _{0.53} As	GRIN	-	3.328
10 nm	Al _{0.22} Ga _{0.29} In _{0.49} As	Barrier	-	3.389
5 × 6 nm	Al _{0.07} Ga _{0.22} In _{0.71} As	Quantum Well	-	3.553
5 × 10 nm	Al _{0.22} Ga _{0.29} In _{0.49} As	Barrier	-	3.389
60 nm	Al _{0.34} Ga _{0.13} In _{0.53} As	GRIN	-	3.328
60 nm	Al _{0.42} Ga _{0.05} In _{0.53} As	Electron confinement	Silicon	3.279
100 nm	InP	Substrate	Silicon	3.146

Table 3.1: Wafer's layers structure

3.2 Waveguide

In optical networks, a waveguide is a basic structure which is used to guide the electromagnetic waves. It is a fundamental element that connects the different parts or devices on a photonic integrated circuit. In this thesis, a dielectric slab waveguide is used for designing all devices. A waveguide could be fabricated either a shallow etched or deep etched. For shallow etched waveguides, an accuracy of the etch depth is required to precisely stop above the core. The main advantage of the shallow etched waveguide is its low sidewall recombination losses. The affiliated drawbacks to this type of waveguides are moderate bending losses and weak horizontal confinement. On the other hand the deep etched waveguide has a strong horizontal optical confinement and extremely low bending losses. Fig. 3.1 illustrates the basic structures of both deep and shallow etched waveguides.

In shallow etched waveguide, the light is confined horizontally by the refractive index difference of etched and non-etched areas of waveguide while the index difference of core-cladding confines the light vertically. Shallow etched waveguide has a great potential where it is needed the sidewall recombination to be minimal. On the other hand, the confined optical mode is very sensitive to the bending losses due to the weak horizontal confinement.

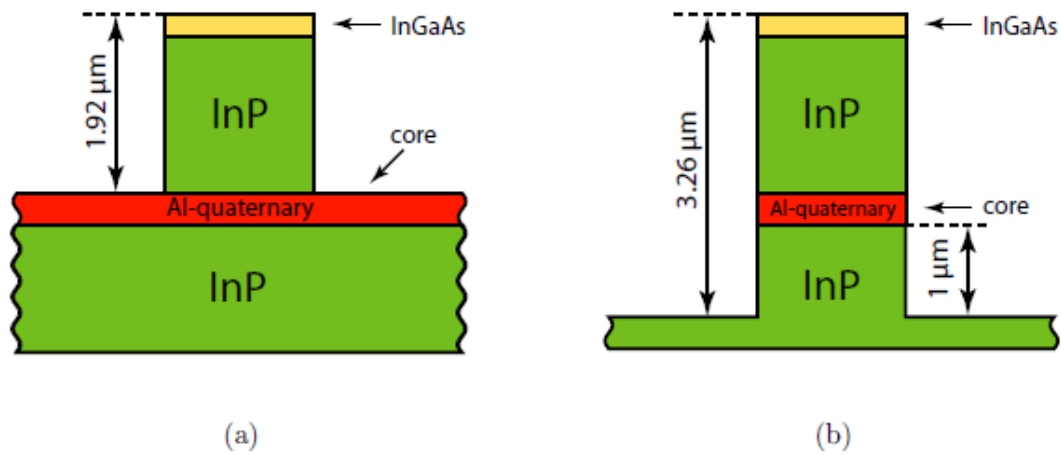


Figure 3.1: Cross section of a) Shallow etched waveguide b) Deep etched waveguide.

In contrast to the shallow etched waveguides, the deep etched waveguide offers a much better horizontal confinement due to the larger index difference between core and air. Because of this, the modal profile becomes more symmetrical and the bending losses are significantly low as compared to the shallow etched design. All the devices presented in this thesis are based on the “deep-etched waveguide”.

3.3 Waveguide Design

During the waveguide designing process, the optimization of its dimensions is a key thing to ensure the existence of a single transverse mode only. Since the etching, in deep etched waveguide, penetrates to the core so the horizontal confinement of the optical wave increases greatly. A beam propagation method (BPM) is used for the initial simulations. The waveguide depth is fixed to 3.2 μm included 1 μm below to the core (*Figure 3.2a*). In *figure 3.2b*, the contour map of the first order transverse mode of the constructed waveguide is shown. It can be shown that the index profile is symmetrical near to the circular which exhibits the less sensitivity for bending losses.

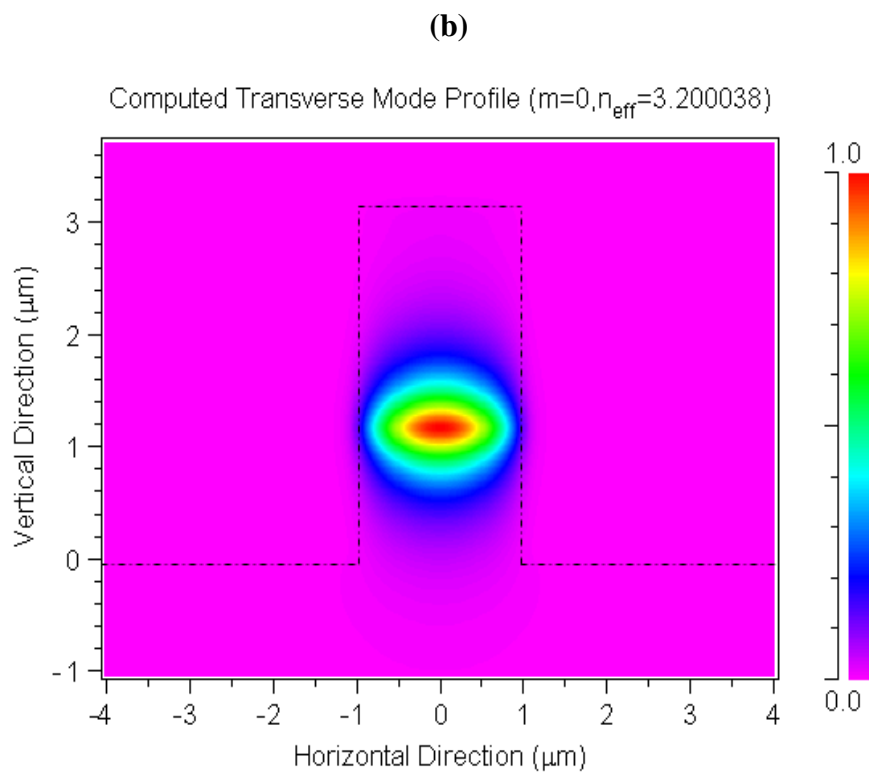
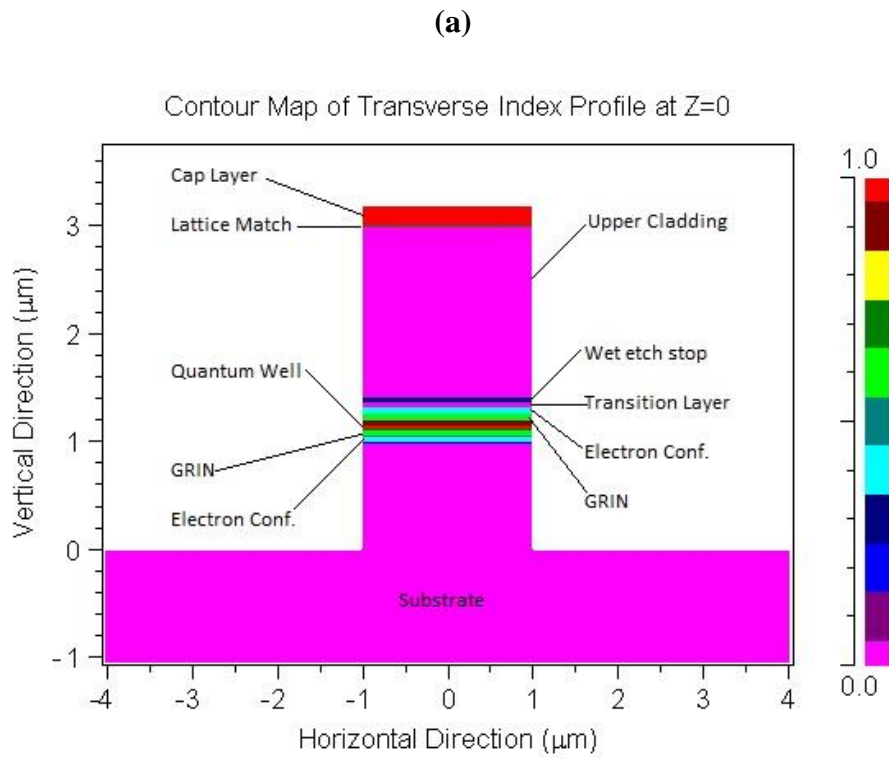


Figure 3.2: a) The constituted $2\ \mu\text{m}$ wide and $3.2\ \mu\text{m}$ deep etched waveguide structure and b) Contour map of TE_{00} mode of the designed deep etched waveguide. Dotted lines indicate the waveguide boundaries.

The simulated effective modal index for the first three TE modes as a function of waveguide width (w) is analysed in *figure 3.3*. Since the horizontal confinement of a deep etched waveguide is much stronger than the vertical confinement so as the waveguide width is reduced the mode is being squeezed horizontally and the optical field expands in vertical direction. This impacts on the substrate losses to be dominant.

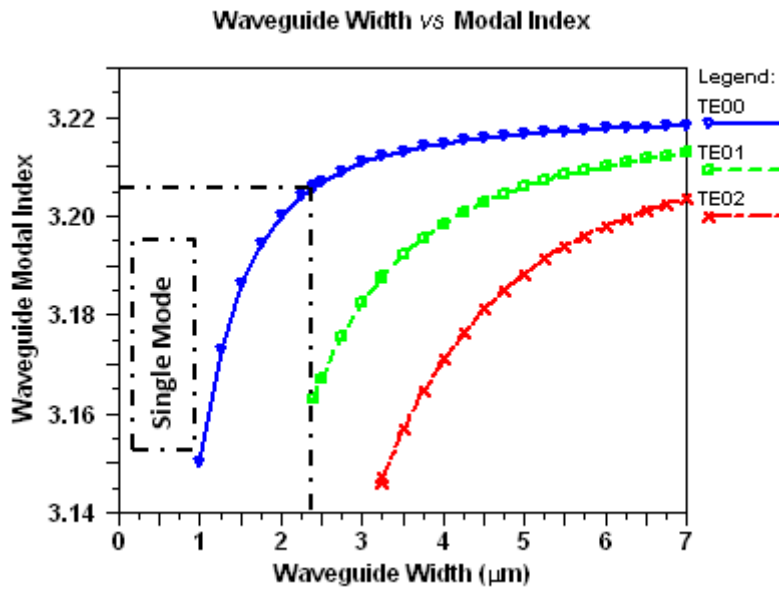


Figure 3.3: Simulated effective index (n_{eff}) for the first three TE modes as a function of waveguide width.

It is realized that the higher order modes are occurred at the larger waveguide width values. The waveguide acts as single mode below the width of $2.4 \mu\text{m}$ and no higher order mode does exist. As per simulations the optimal value of waveguide width for the low loss and the single mode operations ranges from $2 \mu\text{m}$ to $2.4 \mu\text{m}$. Since the size of device is preferred to be compact as it can be possible so a waveguide width of $2 \mu\text{m}$ is chosen for single mode operations in this thesis.

Chapter Summary

In this chapter, the properties of the material which is used to fabricate all the devices of this thesis are discussed. In later sections, the waveguide design along with simulation analysis is carried out. In our case, the waveguide acts as single mode below the width of $2.41 \mu\text{m}$. The upcoming chapter includes the multimode interference coupler design and analysis.

Chapter 4

Multimode Interference Coupler

A multimode interference (MMI) coupler has a wide range of applications in optical communications like splitters, combiners, multiplexers and switches. Depends on the applications, a variety of MMI structures are proposed in the literature. In this chapter, the design of an optimal 3 dB multimode Interference (MMI) Coupler is presented which is further utilized in the formation of a Mach-Zehndar Interferometer.

4.1 Introduction

In any photonic integrated circuit, the splitting, recombining and routing of the optical wave are the vital functions. MMI couplers are considered to be very attractive due to a list of advantages such as fabrication robustness, minimal insertion losses, insensitive to wavelength and polarization, multiple ports and compactness associated with [40]. These are also favourable for the complex devices like Mach-Zehndar Interferometers (MZIs), ring lasers and modulators. The function of the MMI coupler is based on the self-imaging principal which is first proposed by the Bryngdahl [41]. Self-imaging principal states that a number of equivalent images of the input beam are produced along with the coupler length. The number of images, in a row, depends on the width of coupler. So, it is said that there is existing an integral relationship between the propagation constants of various modes.

The dimensions of the multimode interference couplers, while using then into the switch, is determined in next sections of this chapter. The MMI width and length ratio for 3 dB operations are determined by analytically analysing the modal propagation as well as 3-D BPM simulations.

4.2 Self-Imaging & Multimode Interference

It has been analysed in *Chapter 3* that the waveguide becomes multimode above the width of 2.4 μm . So, choosing the appropriate width for multimode operations is based on the

applications where the coupler has to be used. Since, we chose the width of 2 μm for single mode operations such that the access ports of MMI coupler will be 2 μm wide. Thus the minimum width of MMI cavity, to control the reflection of light among adjacent access ports, is 4.25 μm . For our work we are chosen 4.5 μm of width for MMI region based on the optimal level of losses and reflections. At the free waveguide λ , the multimode waveguide has m number of lateral modes with the propagation constants β_i where $i = 0, 1, 2, \dots, (m - 1)$.

Theory of slab waveguide and [42] indicate that both the wavenumber j_{yi} and the propagation constant β_i have a relation to the effective index of waveguide n_{eff} . This relation can be represented with the dispersion equation:

$$n_{eff}^2 j_0^2 = j_{yi}^2 + \beta_i^2 \quad (4.1)$$

Here

$$j_0 = \frac{2\pi}{\lambda_0} \quad (4.2)$$

And

$$J_{yi} = \frac{(i+1)\pi}{W_{eff}} \quad (4.3)$$

Here, W_{eff} is the effective width of the waveguide and represent the Goos-Hanchen shift. This W_{eff} is defined as:

$$W_{eff} \approx W + \frac{\left(\frac{\lambda_0}{\pi}\right)\left(\frac{n_c}{n_{eff}}\right)^{2\sigma}}{\sqrt{n_{eff}^2 - n_c^2}} \quad (4.4)$$

Here, σ indicates the polarization state. $\sigma = 1$ indicates the TM polarization and $\sigma = 0$ represents the TE polarization. By the equations 3.1 – 3.3 and the binomial expansion with $j_{yi}^2 \ll j_0^2 n_{eff}^2$:

$$\beta_i \approx n_{eff} j_0 - \frac{(i+1)^2 \pi \lambda_0}{4 n_{eff} W_{eff}^2} \quad (4.5)$$

The beat length L_π can be specified between the fundamental mode and the first order modes; i.e. ($i=0$) and ($i=1$) respectively. So,

$$L_\pi = \frac{\pi}{\beta_0 - \beta_1} \cong \frac{4n_{eff}W_{eff}^2}{3\lambda_0} \quad (4.6)$$

Thus, the spacing between the propagation constants is:

$$(\beta_0 - \beta_i) \cong \frac{i(i+2)\pi}{3L_\pi} \quad (4.7)$$

By using the mode analysis, Soldano has shown that the input field can be decomposed into many field distributions ψ_i :

$$\Psi(y, 0) = \sum_i c_i \psi_i(y) \quad (4.8)$$

Here, c_i is the coefficient of field excitation which is estimated by the overlap portion of the input beam and decomposed field distributions after taking their integrals i.e. $\Psi(y, 0)$ and $\psi_i(y)$:

$$c_i = \frac{\int \Psi(y, 0) \psi_i(y) dy}{\sqrt{\int \psi_i^2(y) dy}} \quad (4.9)$$

If there exist only the guided modes from the excitation of the input field $\Psi(y, 0)$ then:

$$\Psi(y, 0) = \sum_{i=0}^{m-1} c_i \psi_i(y) \quad (4.10)$$

Equation (4.10) implies that the input field is decomposed into all possible modes in a multimode waveguide.

According to the analysis presented in [42], the field profile can be represented as a linear superposition of Eigen-modes $\psi_i(y)$ at any position along the propagation way in z direction.

$$\Psi(y, z) = \sum_{i=0}^{m-1} c_i \psi_i(y) \exp[k(\omega t - \beta_i z)] \quad (4.11)$$

From equation (4.11), to make the equation time independent the phase of the fundamental mode can be eliminated after taking it as a common factor. Thus the field profile can be derived as:

$$\Psi(y, z) = \sum_{i=0}^{m-1} c_i \psi_i(y) \exp[k(\beta_0 - \beta_i)z] \quad (4.12)$$

At any distance L, the field profile can be obtained by putting equation (4.7) into the equation (4.12):

$$\Psi(y, L) = \sum_{i=0}^{m-1} c_i \psi_i(y) \exp[k(\frac{i(i+2)\pi}{3L_\pi})L] \quad (4.13)$$

It is noted that the images that are formed along the length of multimode waveguide are dependent to the excitation of the input field c_i . Thus the mode phase is equal to:

$$\exp[k(\frac{i(i+2)\pi}{3L_\pi})L] \quad (4.14)$$

In specific conditions, the output field is almost equal to the input field; occurrence of self-imaging. The output field $\Psi(y, L)$ shall be almost a reproduction of the input field $\Psi(y, 0)$ when:

$$\exp[k(\frac{i(i+2)\pi}{3L_\pi})L] = 1 \quad (4.15)$$

OR

$$\exp[k(\frac{i(i+2)\pi}{3L_\pi})L] = (-1)^i$$

It is shown that the both first and second conditions may only be fulfilled when:

$$L = p(3L_\pi); \text{ for } p = 0, 1, 2, \dots \quad (4.16)$$

Here, p denotes the period for the image formulation along the length of waveguide. There would be two situations; either p is even or odd. When p is odd, mirrored images are to be formed and direct images are formed when p is even. (Fig. 4.2).

There would be some images formulated in between the mirrored and direct images at some distances. These distances are:

$$L = \frac{p}{2}(3L_\pi); \text{ Where } p = 1, 3, 5, \dots \quad (4.17)$$

We find that:

$$\Psi(y, \frac{p}{2}(3L_\pi)) = \frac{1+(-k)^p}{2} \Psi(y, 0) + \frac{1-(-k)^p}{2} \Psi(-y, 0) \quad (4.18)$$

According to this condition (Eq. 3.18), two images having the amplitudes $1/\sqrt{2}$ are formed in quadrature at the distances: $z = \frac{1}{2}(3L_\pi), \frac{3}{2}(3L_\pi), \dots$ (Fig. 4.1).

4.3 Multimode Interference Coupler Design

In our work, 2×2 MMI couplers are required to be used in Mach-Zehndar Interferometer. For this case, the two suitable self-imaging regimes in multimode waveguides are: $2 \times N$ restricted paired interference regime and $N \times N$ general interference regime. In first regime the formulated images are depend on the excitation of the input mode while in later one the images are independent from the modal excitation.

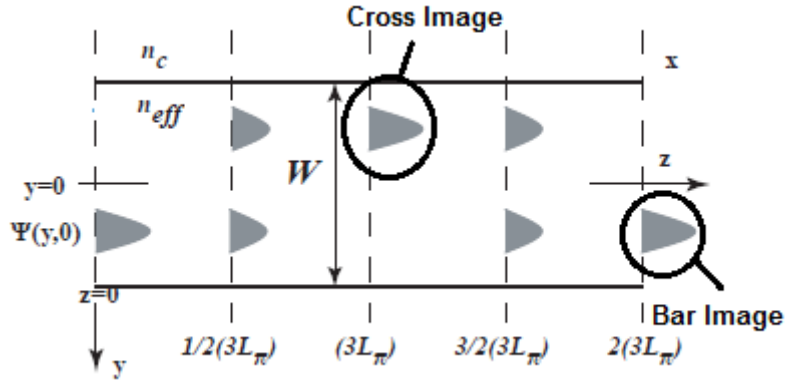


Figure 4.1: Self-imaging properties of multi-mode waveguide.

Usually in $N \times N$ general interference regime self-imaging couplers (Fig. 4.2), the first single image formulates at the distance $3L_\pi$ while the first N -fold image is formed at the distance:

$$L = \frac{3L_\pi}{N} \quad (4.19)$$

Here N denotes the number of input/output ports.

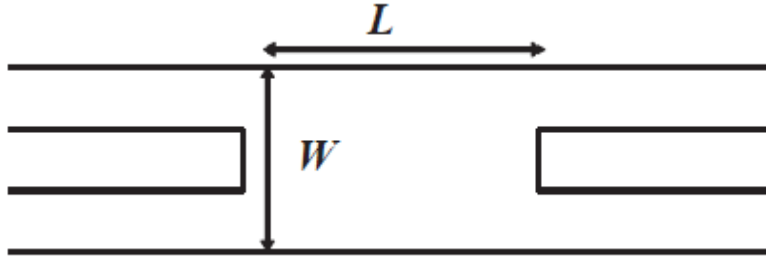


Figure 4.2 Layout of a 2×2 MMI coupler (general interference regime)

Comparing the *general interference regime* to the *restricted paired case* (Fig. 4.3), the first single image is usually found at the length $L\pi$ while the first N-fold image could be formed at:

$$L = \frac{L_\pi}{N} \quad (4.20)$$

During the comparison of both regimes, it seems that the restricted paired regime has the shorter length for a 2×2 MMI coupler. But it is not a matter of fact all the time as it is most likely the length L_π to be differ during the two simulations. It is very important to keep the access waveguides at reasonable distance such that evanescent field coupling is to be avoided between them. If one ignores this factor then the access waveguides (ports) will act as multimode waveguides. So, the distance between the access waveguides should be at least 2 μm for these

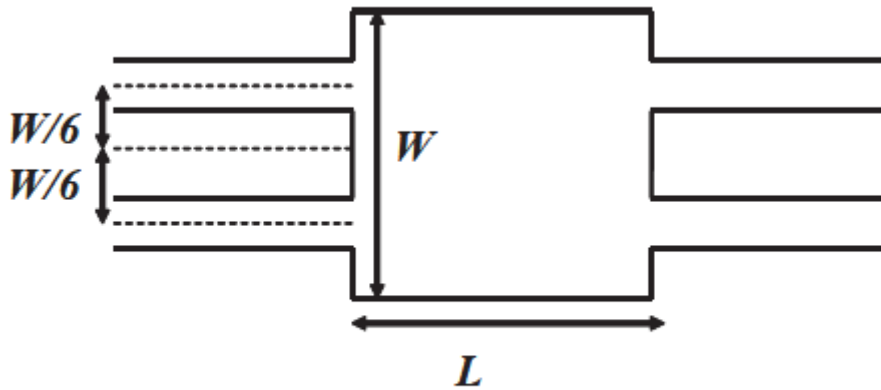


Figure 4.3: 2 × 2 MMI coupler with restricted paired interference regime

kind of devices. In our case the width of the access waveguides is also 2 μm so the restricted paired interference regime requires that the input waveguides are to be located at $+W/6$ & $-W/6$. This implies that the minimum width, W , of MMI region would be about 12 μm . As the *general interference coupler* is free from such kind of restrictions so the allowed width for MMI region would be about 6 μm . So, to keep the device width minimal we chose the general interference couplers in our work.

Since we are working with a 2×2 coupler while keeping the width into account, so we need enough coupler width but to the minimal level that can support not only the two modal images but also provide the flexibility to the access waveguides to remain them single mode waveguides. As it is mentioned earlier (*in chapter 3*), the chosen waveguide width for single mode operations is $2 \mu\text{m}$. So, in order to obtain a two modes coupler a waveguide width of $4.5 \mu\text{m}$ is chosen in this thesis. By inserting the values $W = 4.5$, $n_{\text{eff}} = 3.20$, $n_c = 3.165$ and $\lambda_0 = 1.55$ into the equation (4.4), the effective waveguide width $W_{\text{eff}} \cong 5$ is obtained. Now, the coupler length, that yields the two modes at the output, can be calculated by using the equation (4.19). In our case, this length is calculated to be about $103 \mu\text{m}$. A BPM simulation was performed to verify this calculated result (Fig. 4.4).

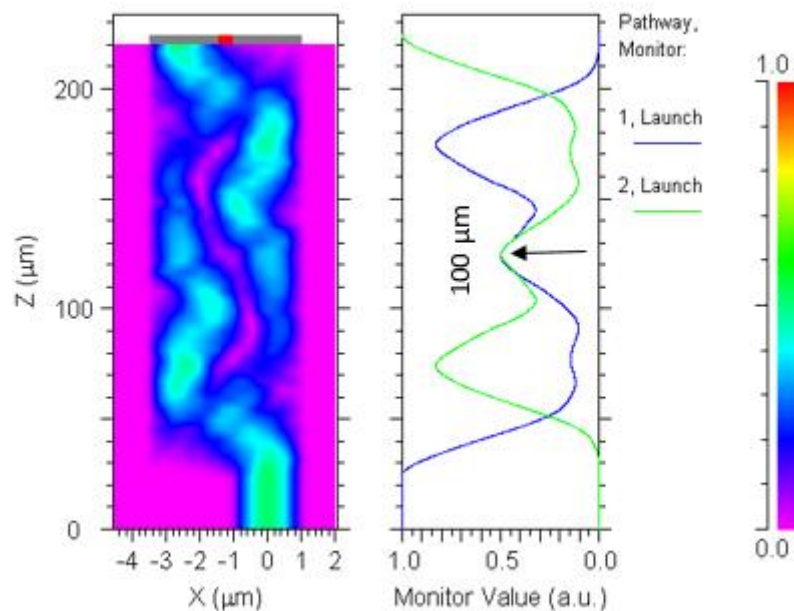


Figure 4.4: A 3-D BPM simulation of general interference coupler having the physical width of $4.5 \mu\text{m}$. It can be shown that the coupling length for 3 dB operation appears at $100 \mu\text{m}$.

In our simulation experiment (Fig. 4.4), it shows the simulated power of the output waveguides. It can be seen that the curves of both output monitors are intersecting each other at the coupler length $100 \mu\text{m}$ that indicates the equal power in both outputs. The difference between the calculated theoretical result and simulation result is about $3 \mu\text{m}$ only. The designed 3 dB coupler with a multimode length of $100 \mu\text{m}$ is shown in *figure 4.5a*.

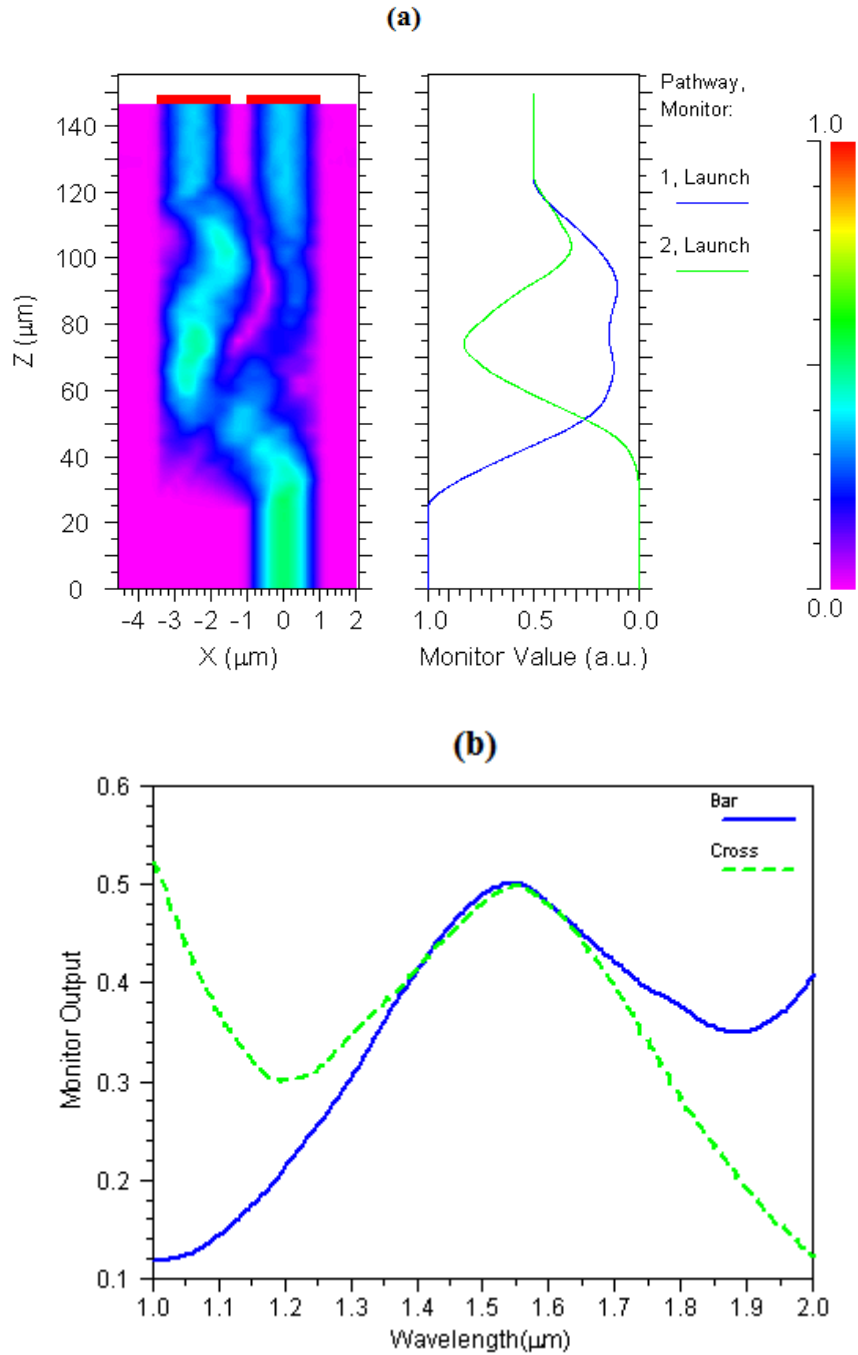


Figure 4.5: a) A 3-D simulation of 3 dB coupler, b) Transmission analysis of the designed 3dB coupler

Figure 4.5b shows the analysis of our designed coupler to be further used in MZI. Since it is designed for the low attenuation transmission window 1550 nm thus the coupler length is also chosen according to the same wavelength. It can be seen that the coupler acts as 3 dB, equal power on both the *cross* and *bar*, at 1550 nm. As the wavelengths window is deviated from the centre wavelength, the transmission is also being deviated.

Chapter Summary

In this chapter, a 3 dB multimode interference coupler is designed to be used in the constitution of MZI. Further, the working principle of MMI coupler, self-imaging, is also analysed. The designed coupler exhibits the transmission losses as low as 0.0108 dB for the 1550 nm transmission window. At 1550 nm, the coupler performs as a 3 dB splitter which is the requirement of MZI. In next chapter, the Mach-Zehnder Interferometer (MZI) switch is formulated and analysed.

Chapter 5

Mach-Zehnder Interferometer for optical switching

In previous chapters, the components that are required to assemble the structure of a Mach-Zehnder Interferometer switch have been presented. In this chapter the previously designed components are assembled to construct the optical switch. In later sections of this chapter, the simulation results are carried out to measure the switch performance.

5.1 Introduction

An optical switch plays a vital role in optical communications to perform the routing of optical signals independent to data protocol and data rate. It enables the optical signals in photonic integrated circuits or optical fibres to be selectively switched from one port to another or from one fibre to the other fibre. The applications for such type of switching devices range from access networks to back-haul networks. MZIs type photonic integrated circuits are very attractive for wavelength conversion [43], high speed optical switching [44] and wavelength (de)multiplexing operations [45].

A Mach-Zehnder Interferometer type switching circuit consists of two 3 dB couplers which are connected through the two arms. The first coupler split the input signal power into two equal power images which are transmitted to the second coupler through the different arms. Second coupler, then, recombines the two incoming signals to be routed on one of its output ports. The change in refractive index of one of the two arms causes the change of phase such that the optical signal is to be switched from one port to the other.

The applications of the optical switches require the circuits with low crosstalk and losses while supporting to the larger amount of wavelengths. In addition to these basis function requirements, some additional requirements like manufacturability and the device size could

also be imposed. The higher level of fabrication tolerance and small circuit size are considered as inexpensive and easy way of a switch fabrication.

5.2 Switch Design

In our design, two 3 dB MMI couplers are adjoined through two passive waveguides called as arms. A monolithically integrated active phase shifter is also placed in one of the arms to change the refractive index for obtaining the appropriate phase shift at the output coupler. The important parameters on which the performance of the switch will be analysed are *crosstalk*, *end-to-end losses* & *bandwidth support*.

It is very important to minimize the losses of an integrated circuit that the waveguides which are used to construct the circuit must be carefully designed such that they exhibit low losses. The chosen waveguides should have negligible bending losses and have sufficient space between adjacent ports to align the optical fibre on input and output ports. Also it is vital the couplers are to be designed correctly with minimal imbalance factor at output ports as the greater the power imbalance lows the extinction ratio in a MZI. The MMI couplers are an attractive choice to be used in MZIs due to their wavelength insensitivity, polarization insensitivity and stable balance.

In this thesis, deep etched wave-guiding structure and MMI couplers, explained in chapters 3 and 4 respectively, are used to realize a 2×2 MZI. The device layout is shown in figure 4.1. It consists of two input port In_1 and In_2 and two output ports Out_1 and Out_2 . The light enters in one of two input ports is guided through first coupler which acts as a splitter. Since the employed coupler is designed for 3 dB operations, it splits the light beam into two equal power images as described in chapter 3. Now the output of this splitter is transmitted in two different arms which are eventually reached at the second coupler. This second coupler received two inputs from the both of input arms and combine them through the principle of constructive interference onto one of its output ports.

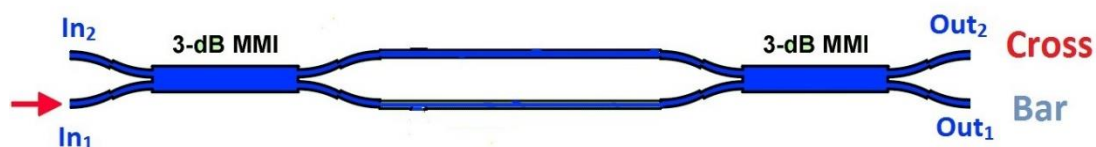


Figure 5.1: Schematic structure of Mach-Zehnder Interferometer based optical switch

In simple MZI structure (*fig. 5.1*), if there is not added any additional phase difference then the second coupler, equivalent to the first coupler, receives two input signals with a $\pi/2$ phase difference. This states that a constructive interference shall be occurred on one of the two output ports and a destructive interference on the other port. It is observed that the maximum power of the optical signal will be on “*Cross*” port; a so called “*Cross State*”. In our experiments, we observed this output power as high as 0.0177 dB with respect to the input power. The graphical representation of “*Cross State*” is shown in *figure 4.2a*.

On the other hand, if there is imposed an extra phase difference of π then at the input of the second MMI coupler, the phase difference is opposite to the case of “*Cross State*”. Hence, a destructive interference of the light is occurred at the “*Cross*” port and constructively interfere at the other. This is named as “*Bar State*”. The graphical representation of this phenomenon is shown in *figure 5.2b*.

It has been realized that by imposing a phase difference of π , the output port can be switched. The required phase difference could be imposed by changing the refractive index of one of the MZI arms. It has been demonstrated that the additional phase difference can be obtained by changing the refractive index in one or both arms of the MZI [46] – [48]. For this purpose, an active phase shifter is placed on one arm. This phase shifter, when turned on, injects the current in selected portion which causes to increase the effective refractive index of the waveguide. Consequently, the light that passed through this waveguide will reach to the second coupler of MZI with a difference of phase.

Length of the MZI arms plays a vital role in phase shifting. In case where the phase change is achieved through the current injection mechanism, the length of the arms and current density are inversely proportional to each other such that if the length of arms are reduced then the required current density for effective index change is increased. This is a decisive point for the dimensions of the circuit. In our work, we tried to balance the both factors; current density and circuit size. So, we set the length of MZI arms to $400\ \mu\text{m}$.

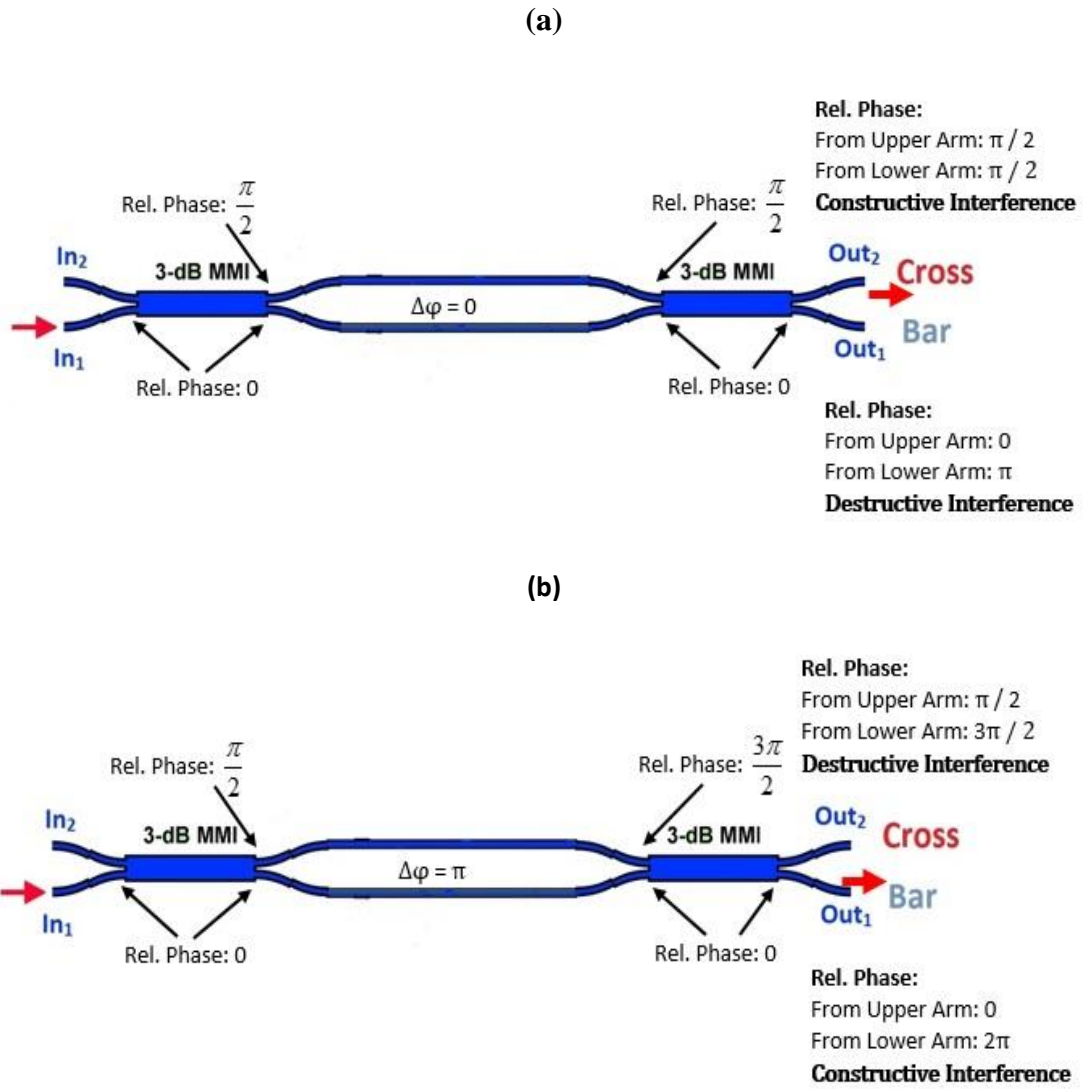


Figure 5.2: Graphical representation of a) cross state b) bar state

In order to obtain the required phase difference, we analysed the cross to bar switching with respect to the current density. A 3-D BPM simulation is carried by placing an electrode (phase shifter) with forward biased DC on the top surface of a straight waveguide and record the impact of current density on the effective index of waveguide. The used phase shifter, in our design, is $2 \mu\text{m}$ wide and $400 \mu\text{m}$ long on the waveguide of same dimensions.

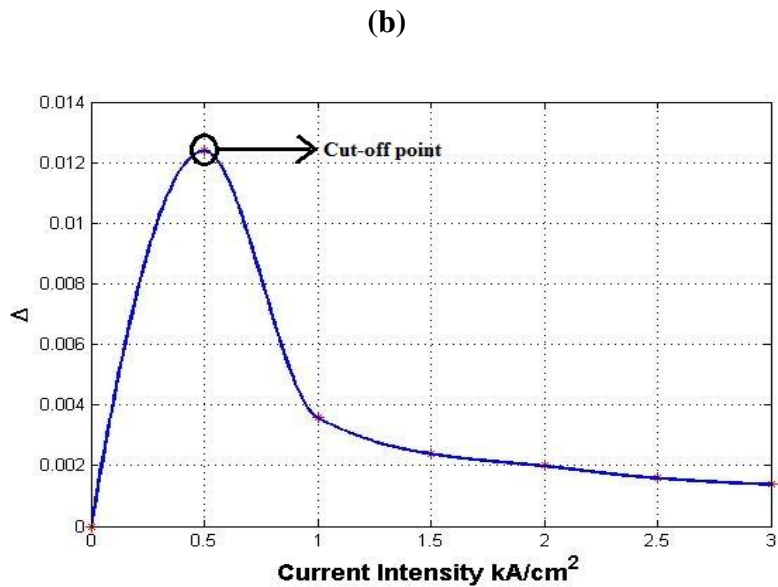
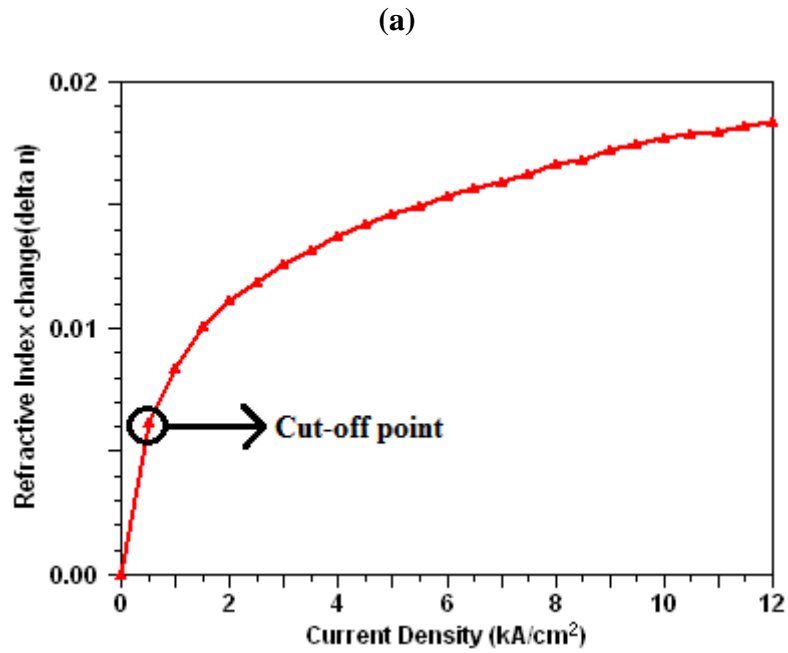


Figure 5.3: a) Impact of current density on effective index of waveguide b) Effective rate of change with respect to the current density

Fig. 5.3a is plotted from the simulation results of PHOTON DESIGN's PICWAVE. PICWAVE has integrated an advanced laser diode and SOA model along with the photonic integrated circuit design tool. This combination allows a user to model the circuits that have both active and passive components. In our experiments, we used to design a 2 μm wide waveguide on which an active electrode of the same width was placed. This electrode behaves actively according to the intensity of current which is to be imposed onto waveguide. The effective index is increased as the forward biased current is employed to the waveguide (*fig. 5.3a*). The rate of change in effective index is geared-up initially as the current employed. By

taking the derivative of this data (fig 5.3a) the cut-off point could be find where on above to that point the rate of change becomes degraded gradually. In our case, above to the intensity of 0.5 kA/cm^2 , the rate of index change is decreased (fig. 5.3b). So, the cut-off current value in our case is 0.5 kA/cm^2 .

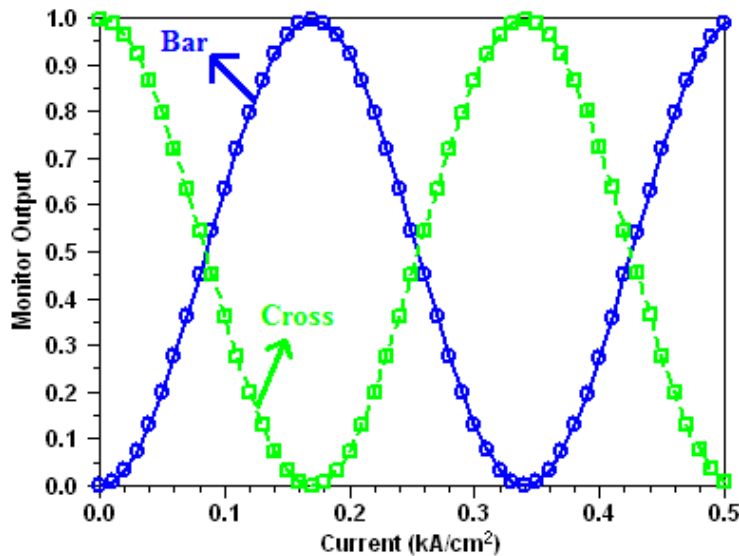


Figure 5.4: Output ports switching with respect to current intensity

Transmission at output ports is switched with respect to the current intensity; as shown in *figure 5.4*. Without imposing any current, the switch acts as *cross state*. As the DC biased current is imposed through the phase shifter in one of the MZI arms, the transmission on output port is started to be switched to *bar port*. At the current intensity of 0.17 kA/cm^2 , the cross state is switched to the bar state.

5.3 Results and Discussion

The designed device is analysed for different wavelengths while the tunings is performed by active electrode on one of the MZI arms. The tuning is performed as a function of current density. Since the index rate of change is being decreased above the value of 0.5 kA/cm^2 so we carried the tuning within this range.

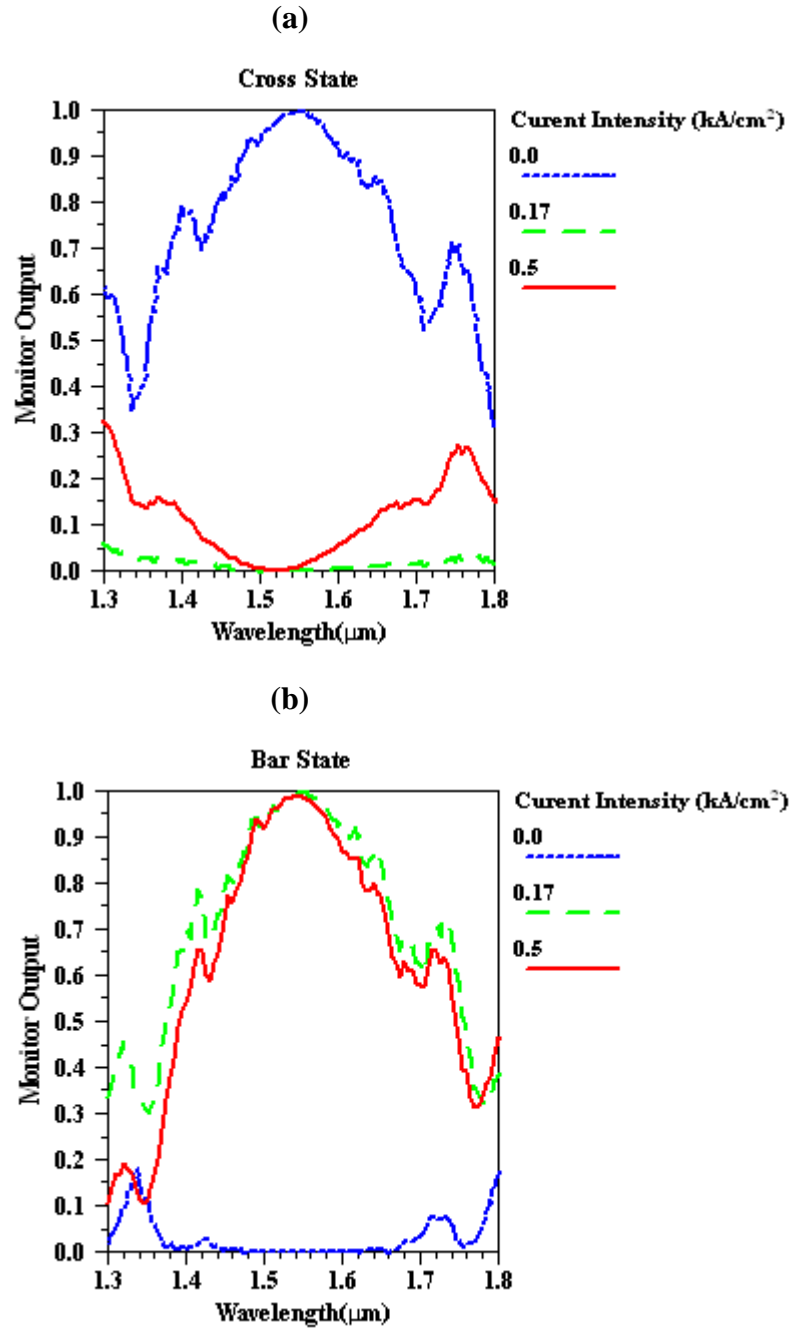
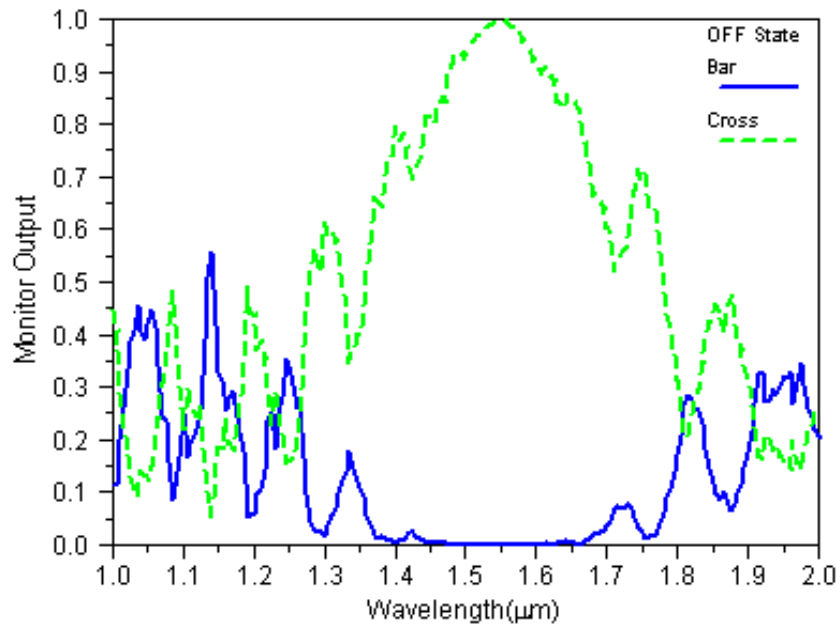


Fig. 5.5: Transmission window along with different tuning impacts a) cross state b) bar state

The designed switch is normally acts as “*cross state*”. As the current injected into one of the MZI arms, the effective index of the waveguide portion is increased. This causes an additional phase difference of π with respect to the other MZI arm, when the optical beam reached to the second MMI coupler. As a consequence, the optical power on the “*cross*” is start to be decreased due to the destructive interference on cross port. On the other hand, a constructive interference is start to be occurred on “*bar*” port. The first switching cycle is completed by employing the forward biased DC of the intensity 0.17 kA/cm^2 (figure 5.5).

(a)



(b)

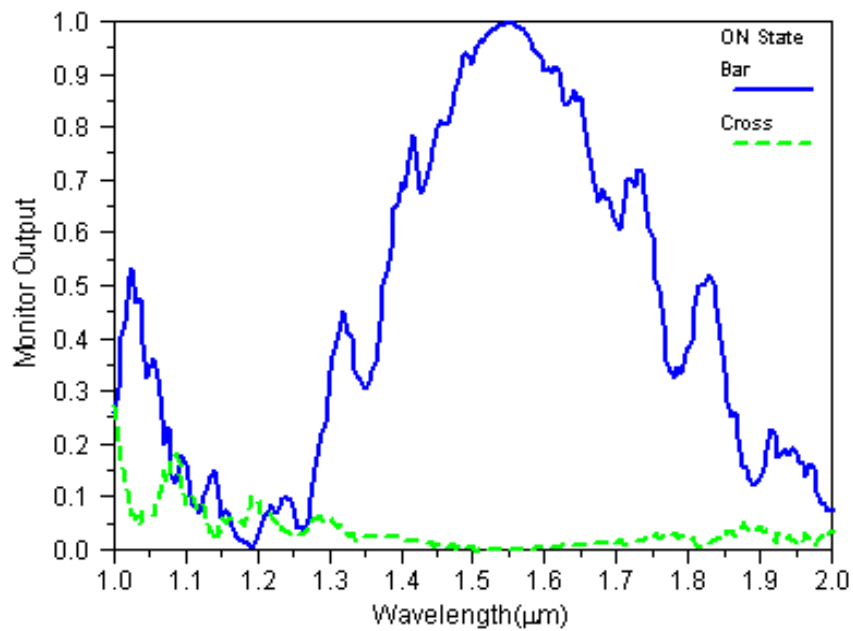


Figure 5.6: Transmission of both switch states a) OFF state b) ON state

From the operational point of view, the designed switch can be categorized in two states; *OFF state* and *ON state*. An off state indicates that the switch is functional as cross state and no

current is launched into the phase shifter. In such case, the transmission is carried out through the cross port as shown in *figure 5.6a*. On the other hand when it is needed to switch the output port from *cross* to *bar* then the current is employed through the active diode (so called phase shifter). Although the wavelength tuning could be viable till the current intensity of 0.5 kA/cm^2 in our case but the out port is shifted to the *bar* from the *cross* by employing a current intensity of 0.17 kA/cm^2 ; as shown in *figure 5.6b*.

The losses incorporated to the designed circuit are as low as 24 dB. In 3-D BPM simulation, a FWHM bandwidth of 390 nm is achieved which supports the entire transmission window of 1550 nm.

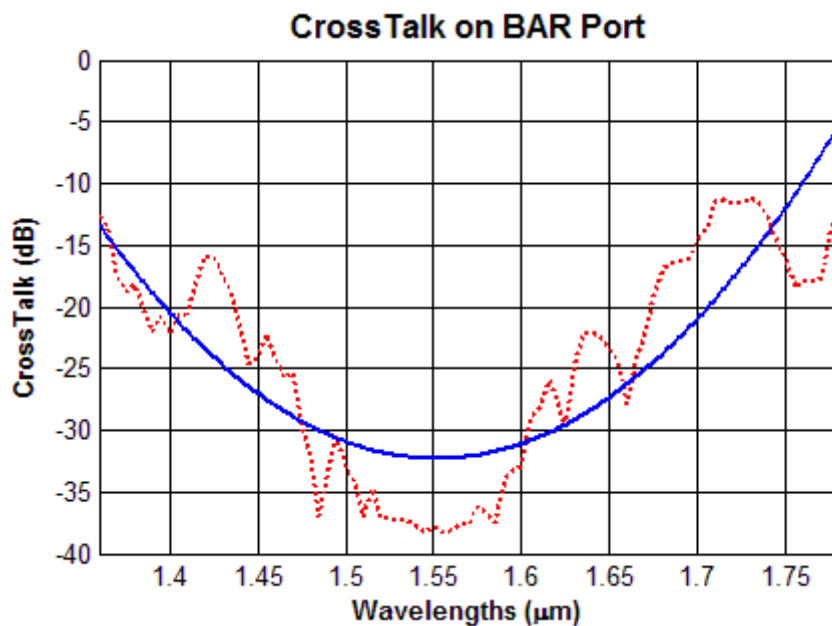


Figure 5.7: Crosstalk on BAR when switch is on cross state

Crosstalk is an important factor when a photonic integrated circuit has to be designed. It could be measured as:

$$Crosstalk = 10 \log \left(\frac{P_3}{P_4} \right) \quad (5.1)$$

Where P_3 and P_4 are the output ports of the switch. When the switch is in OFF state then the crosstalk will be calculated on *bar* port while it will be measured on *cross* port when the switch is in ON state. In our case, the observed crosstalk level on the bar port is -38 dB which is further reduced significantly when the switch is in ON state. (*Figures 5.7 and 5.8*)

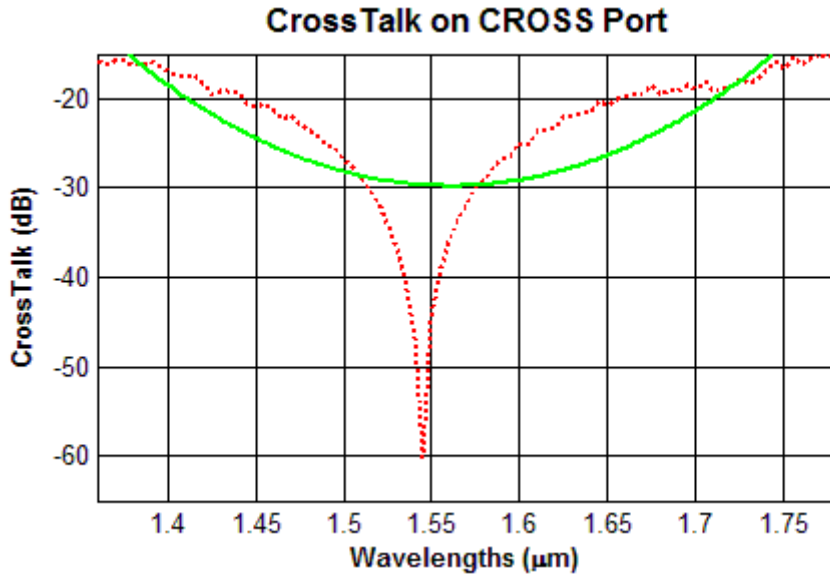


Figure 5.8: Crosstalk on BAR when switch is on cross state

5.4 Comparison with reference paper

A comparative study is carried out to validate the results of our device. For this purpose the research publication of H.Y. Wong [44] is chosen as the function methodology of our device and the said publication is same. A multiple quantum well structure of the material InGaAs–InAlGaAs is used in [44] where the selected waveguide width for single mode operations is 2 μm wide which is same for our case too. The designed coupler in this thesis has the dimensions of $4.5 \times 100 \mu\text{m}$ while the coupler that is proposed in reference publication has the dimensions of $6 \times 220 \mu\text{m}$. Both of devices are formulated to be worked on the central wavelength 1550 nm. The MZI switch [44] has an experimental bandwidth of about 120 nm (1460 – 1580 nm) while our designed switch exhibits a FWHM bandwidth of about 390 nm (1370 – 1760 nm).

Both of the switches, [44] and our designed, has the 400 μm long MZI arms on which active phase shifters are to be placed. The MZI switch [44] completes the first switching cycle with a current injection of about $\sim 3.5 \text{ mA}$ (*figure 5.9*) while in our case the required current density is about 0.17 kA/cm^2 (about $\sim 3.6 \text{ mA}$); *figure 5.4*. Hence, the current efficiency of [44] is better than our designed circuit but with the trade-off of the requirement of an extra phase-shifter. Our designed MZI switch has only one active phase shifter in one of its arms while the reference device has two phase shifters in both of its arms. During the wavelength tuning process, both the active phase shifters are used simultaneously.

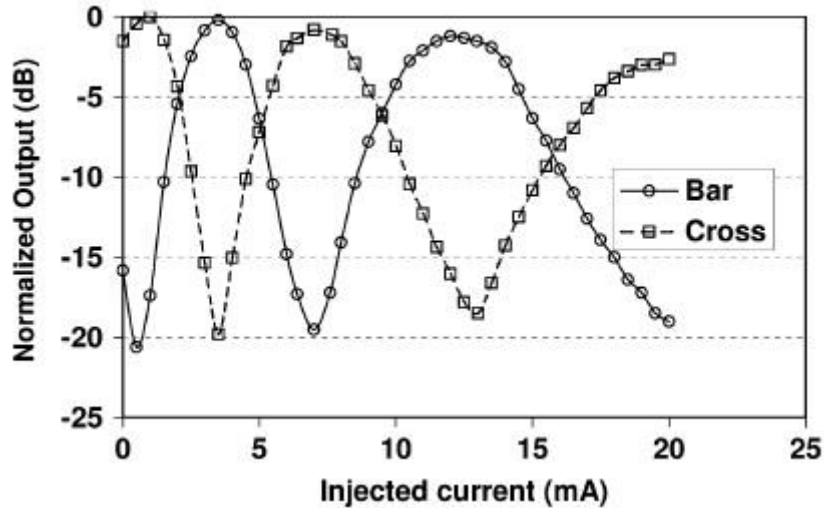


Figure 5.9: The switching characteristics of the MZI switch with respect to the injected current. [44]

The reported transmission loss of the circuit [44] is 19 dB while it is reduced to 24 dB in our case. The obtained crosstalk level in reference device is as low as -20 dB while it is reduced in our switch to a level of -38 dB.

Chapter Summary

In this chapter a Mach-Zehnder Interferometer (MZI) based switch is designed and analysed. The designed circuit could be used in time asynchronous optical networks for switching and or multiplexing operations. The device analysis is carried out by using a 3-D Beam Propagation Method. The formulated device offers the bandwidth of 390 nm on the central wavelength 1550 nm. The transmission loss is as low as 24 dB while the achieved crosstalk level is as low as -38 dB.

Chapter 6

Conclusion and Future work

6.1 Thesis Summary

Optical networks are the key to high speed communication and solution to the bandwidth limitations. Especially WDM networks are really a revolution in the era of optical communications. In an optical network, there is a list of components that makes the optical transmission viable. An optical switch is one of these components that is used to selectively switch the output ports.

The core of this thesis is to design an optical switch that bases on Mach-Zehnder Interferometer (MZI). The chosen material for the fabrication of circuit is AlGaInAs multiple quantum well (MQW). The waveguide is etched to a depth of 3.2 μm . According to our analysis, the waveguide acts as single mode below the width of 2.41 μm . To keep the device size minimal, we used the waveguide width of 2 μm for single mode operations.

The MMI cavity is designed by taking the waveguide width of 4.5 μm such that it can be supported the two input and two output waveguides of single mode without disturbing the single mode operations. The coupler has a coupling length of about 100 μm that is optimized through parametric simulations. On the wavelength of 1550 nm, the coupler acts as a 3 dB splitter.

Two MMI couplers are connected together via a pair of straight waveguides to formulate the Mach-Zehnder Interferometer device; so called MZI arms. In one of these arms, an active phase shifter is placed for wavelength tuning and output port switching purpose by injecting the biased DC through it. When the switch is in OFF state the, the transmission is carried out on cross port. The ON state switches the transmission from cross to bar port.

The obtained bandwidth for the designed circuit is about 390 nm. The observed transmission loss is as low as 24 dB while the crosstalk level is below -38 dB. The tool used for optical components design and simulation is RSoft BeamPROP.

6.2 Future Work

We analysed a 2×2 optical switch on the basic metrics bandwidth, transmission loss and crosstalk. A further analysis for the same circuit on other performance metrics can be performed as a future plan; switching response time, extinction ration and polarization (in) dependency. The fabrication tolerance of the switch may be analysed in future.

The current circuit routes the optical power between two out ports. Depending on the network scenario, more switching options may be required to be incorporate with. So as a future work option, the switch structure with more than two out ports may be formulated.

References

- [1] T.H. Maiman, "Stimulated optical radiation in ruby", *Nature*, vol. 187, pp. 493 - 494, 1960
- [2] F.P. Kapron, D.B. Keck and R.D. Maurer, "Radiation losses in glass optical waveguides", *Appl. Phys. Lett.*, vol. 17, pp. 423 - 425, 1980
- [3] H.J.R. Dutton, "Understanding Optical Communications", Upper Saddle River, Prentice Hall, 1998
- [4] L.G. Kazovsky, S. Benedetto and A.E. Willner, *Optical Fiber Communication Systems*, Norwood, Artech House, 1996
- [5] S. Kawanishi, H. Takara, K. Uchiyama, I. Shake and K. Mori, "3 Tbit/s (160 Gbit/s*19ch) OTDM/WDM transmission experiment", *Proc. OFC/IOOC'99*, 1999
- [6] S. Johansson, "Transport network involving a reconfigurable WDM network layer-a European demonstration", *IEEE J. Lightw. Technol.*, Vol. 14, No. 6, pp. 1341 - 1348, 1996
- [7] C.G.P. Herben, C.G.M. Vreeburg, D.H.P. Maat, X.J.M. Leijtens, M.K. Smit, F.H. Groen, J.J.G.M. van der Tol and P. Demeester, "A compact integrated InPbased single-PHASAR optical crossconnect", *IEEE Photon. Technol. Lett.*, Vol. 10, No. 5, pp. 678 - 680, 1998
- [8] L.Y. Lin, E.L. Goldstein and R.W. Tkach, "Free-space micromachined optical switches with submillisecond switching time for large-scale optical crossconnects", *IEEE Photon. Technol. Lett.*, Vol. 10, No. 4, pp. 525 - 527, 1998
- [9] D. Bishop, "Silicon Micromachines for Lightwave Networks", *Integrated Photonics Research*, OSA Technical Digest series, pp. 313 - 314, 1999
- [10] M. Tachikura, T. Katagiri and H. Kobayashi, "Strictly nonblocking 512×512 optical fibre matrix switch based on a three-stage cros network", *IEEE Photon. Technol. Lett.*, Vol. 6, No. 6, pp. 764 - 766, 1994

- [11] M. Renaud, I. Privat, J.P. Hébert, J. Le Bris, J.L. Peyre, A. Piquier and J.F. Vinchant, "High speed multifunctional InP module for optical signal processing", Proc. ECOC '94, Firenze, Italy, pp. 515 – 518, Sept. 25–29, 1994
- [12] T. Uitterdijk, Integrated electro-optical switches on InP, Ph.D. Thesis, Delft University of Technology, Delft, The Netherlands, 1997
- [13] E.J. Murphy, T.O. Murphy, A.F. Ambrose, R.W. Irvin, B.H. Lee, P. Peng, G.W. Richards and A. Yorinks, "16 × 16 strictly nonblocking guided-wave optical switching system", IEEE J. Lightw. Technol., Vol. 14, No. 3, pp. 352 - 358, 1996
- [14] R. Krähenbühl, "Electro-optic space switches in InGaAsP/InP for optical communication", Konstanz, Hartung-Gorre, 1998
- [15] F. Kappe, G.G. Mekonnen, C. Bornholdt, F.W. Reier and D. Hoffman, "35 GHz bandwidth photonic space switch with travelling wave electrodes on InP", Electron. Lett., Vol. 30, No. 13, pp. 1048 - 1049, 1994
- [16] M.M. Howerton, R.P. Moeller, A.S. Greenblatt and R. Krähenbühl, "Fully packaged, broad-band LiNbO₃ modulator with low drive voltage", IEEE Photon. Technol. Lett., Vol. 12, No. 7, pp. 792 - 794, 2000
- [17] D.A.B. Miller, D.S. Chemla, T.C. Damen, A.C. Gossard, W. Wiegmann, T.H. Wood and C.A. Burrus, "Bandedge Electro-absorption in quantum well structures: The quantum confined stark effect", Phys. Rev. Lett., Vol. 53, pp. 2173 - 633, 1984
- [18] A. Sneh, J.E. Zucker, B.I. Miller and L.W. Shulz, "Polarization-insensitive InPbased MQW digital optical switch", IEEE Photon. Technol. Lett., Vol. 9, No. 12, pp. 1589 - 1591, 1997
- [19] B.H.P. Dorren, A.Y. Silov, M.R. Leys, D.M.H. Dukers, J.E.M. Haverkort, D.H.P. Maat, Y. Zhu, F.H. Groen and J.H. Wolter, "A chopped quantum well polarization independent interferometric switch at 1.53 μm", IEEE J. Quantum Electron., Vol. 36, No. 3, pp. 317 - 324, 2000
- [20] M. Kohtoku, K. Kawano, S. Sekine, H. Takeuchi, N. Yoshimoto, M. Wada, T. Ito, M. Yanagibashi, S. Kondo, Y. Noguchi and M. Naganuma, "High-speed InGaAlAs-InAlAs

- MQW directional coupler waveguide switch modules integrated with a spotsizer converter having a lateral taper, thin-film core, and ridge”, *IEEE J. Lightw. Technol.*, Vol. 18, No. 3, pp. 360 - 369, 2000
- [21] M. Bachmann, M. Renaud, H.P. Nolting and M. Gravert, “Crosstalk-reduced DOS with high fabrication tolerances designed for InGaAsP / InP”, *Proc. ECOC '96, 22nd European Conference on Optical Communication*, Vol. 3, pp. 261 – 264, 1996
- [22] G. Wenger, M. Schienle, J. Bellermaun, M. Heinbach, S. Eichinger, J. Müller, B. Acklin, L. Stoll and G. Müller, “A completely packaged strictly nonblocking 8×8 optical matrix switch on InP/InGaAsP”, *IEEE J. Lightw. Technol.*, Vol. 14, No. 10, pp. 2332 - 2337, 1996
- [23] M.N. Kahn, B.I. Miller, E.C. Burrows and C.A. Burrus, “Crosstalk-, loss-, and length-reduced digital optical y-branch switches using a double-etch waveguide structure”, *IEEE Photon. Technol. Lett.*, Vol. 11, No. 10, pp. 1250 - 1252, 1999
- [24] N. Yoshimoto, Y. Shibata, S. Oku, S. Kondo and Y. Noguchi, “Design and demonstration of polarization-insensitive Mach-Zehnder switch using a lattice-matched InGaAlAs/InAlAs MQW and deep-etched high-mesa waveguide structure”, *IEEE J. Lightw. Technol.*, Vol. 17, No. 9, pp. 1662 - 1669, 1999
- [25] E.J. Murphy, C.T. Kemmerer, D.T. Moser, M.R. Serbin, J.E. Watson and P.L. Stoddard, “Uniform 8×8 lithium niobate switch arrays”, *IEEE J. Lightw. Technol.*, Vol. 13, No. 5, pp. 967 - 970, 1995
- [26] W.K. Burns, M.M. Howerton, R.P. Moeller, R. Krähenbühl, R.W. McElhanon and A.S. Greenblatt, “Low drive voltage, broad-band LiNbO₃ modulators with and without etched ridges”, *IEEE J. Lightw. Technol.*, Vol. 17, No. 12, pp. 2551 - 2555, 1999
- [27] P. Granstrand, B. Lagerström, P. Svensson, H. Olofsson, J.-E. Falk and B. Stoltz, “Pigtailed tree-structured 8×8 LiNbO₃ Switch Matrix with 112 digital optical switches”, *IEEE Photon. Technol. Lett.*, Vol. 6, No. 1, pp. 71 - 73, 1994
- [28] M. Renaud, M. Bachmann and M. Erman, “Semiconductor optical space switches”, *IEEE J. Sel. Topics Quantum Electron.*, Vol. 2, No. 2, pp. 277 - 288, 1996

- [29] A. Borreman, T. Hoekstra, M. Diemeer, H. Hoekstra and P. Lambeck, "Polymeric 8×8 optical switch matrix", Proc. ECOC '96, pp. 5.59 - 5.62, 1996
- [30] N. Keil, H.H. Yao and C. Zawadzki, "Polymer waveguide optical switch with <-40 dB polarisation independent crosstalk", Electron. Lett., Vol. 32, No. 7, pp. 655 - 657, 1996
- [31] T. Goh, A. Himeno, M. Okuno, H. Takahashi and K. Hattori, "High-extinction ratio and low-loss silica-based 8*8 strictly nonblocking thermo-optic matrix switch", IEEE J. Lightw. Technol., Vol. 17, No. 7, pp. 1192 - 1199, 1999
- [32] D.A. Smith, R.S. Chakravarthy, Z. Bao, J.E. Baran, J.L. Jackel, A. d'Alesandro, D.J. Fritz, S.H. Huang, X.Y. Zou, S.M. Hwang, A.E. Willner and K.D. Li, "Evolution of the acousto-optic wavelength routing switch", IEEE J. Lightw. Technol., Vol. 14, No. 6, pp. 1005 - 1019, 1996
- [33] J.L. Jackel, M.S. Goodman, J. Gamelin, W.J. Tomlinson, J. Baran, C.A. Brackett, D.J. Fritz, R. Hobbs, K. Kissa, R. Ade and D.A. Smith, "Simultaneous and independent switching of 8-wavelength channels with 2-nm spacing using a wavelength-dilated acousto-optic switch", IEEE Photon. Technol. Lett., Vol. 8, No. 11, pp. 1531 - 1533, 1996
- [34] S. Nakamura, Y. Ueno, K. Tajima, J. Sasaki, T. Sugimoto, T. Kato, T. Shimoda, M. Itoh, H. Hatakeyama, T. Tamanuki and T. Sasaki, "Demultiplexing of 168-Gb/s data pulses with a hybrid-integrated symmetric Mach-Zehnder all-optical switch", IEEE Photon. Technol. Lett., Vol. 12, no. 4, pp. 425 - 427, 2000
- [35] J. Leuthold, P.-A. Besse, E. Gamper, M. Dülk, S. Fischer, G. Guekos, H. Melchior, "All-optical Mach-Zehnder interferometer wavelength converters and switches with integrated data- and control-signal separation scheme", IEEE J. Lightw. Technol., Vol. 17, No. 6, pp. 1056 - 1065, 1999
- [36] T. Higashi, S. Sweeney, A. Phillips, A. Adams, E. O'Reilly, T. Uchida and T. Fujii, "Observation of reduced nonradiative current in 1.3 μm AlGaInAs/InP strained MQW lasers," IEEE Photon. Technol. Lett., Vol. 11, No. 4, pp. 409 - 411, 1999
- [37] M. Camargo Silva, J. Sih, T. Chou, J. Kirk, G. Evans and J. Butler, "1.3 μm strained MQW AlGaInAs and InGaAsP ridge-waveguide lasers-a comparative study," in Microwave and

- Optoelectronics Conference. SBMO/IEEE MTT-S, APS and LEOS – IMOC'99. International, vol. 1, pp. 10 - 12, 1999
- [38] Y. Kuo, S. Yen, M. Yao, M.-L. Chen and B. Liou, "Numerical study on gain and optical properties of AlGaInAs, InGaAs, and InGaAsP material systems for 1.3 μm semiconductor lasers," *Opt. Commun.* Vol. 275, No. 1, pp. 156 - 164, 2007
- [39] G. Mezosi, "Semiconductor ring lasers for all-optical signal processing", Ph.D Thesis, Page (35-36), University of Glasgow, August 2010
- [40] P. Besse, M. Bachmann, H. Melchior, L. Soldano and M. Smit, "Optical bandwidth and fabrication tolerances of multimode interference couplers," *Lightw. Technol. J.*, Vol. 12, No. 6, pp. 1004 - 1009, 1994
- [41] O. Bryngdahl, "Image formation using self-imaging techniques," *J. Opt. Soc. Am.*, Vol. 63, No. 4, pp. 416 - 419, 1973 [Online]. Available:
<http://www.opticsinfobase.org/abstract.cfm?URI=josa-63-4-416>
- [42] L. Soldano and E. Pennings, "Optical multi-mode interference devices based on self-imaging: principles and applications," *Lightw. Technol. J.*, Vol. 13, No. 4, pp. 615 -627, 1995
- [43] T. Durhuus, C. Joergensen, B. Mikkelsen, R. Pedersen and K. Stubkjaer, "All optical wavelength conversion by SOA's in a Mach-Zehnder configuration," *Photon. Technol. Lett., IEEE*, Vol. 6, No. 1, pp. 53 - 55, 1994
- [44] H. Wong, M. Sorel, A. Bryce, J. Marsh and J. Arnold, "Monolithically integrated InGaAs-AlGaInAs Mach-Zehnder interferometer optical switch using quantum-well intermixing," *Photon. Technol. Lett., IEEE*, Vol. 17, No. 4, pp. 783 - 785, 2005
- [45] Q. Lai, M. Lanker, W. Hunziker and H. Melchior, "Tunable wavelength selection switch and multiplexer/demultiplexer based on asymmetric silica on-silicon Mach-Zehnder interferometer," *Electron. Lett.*, Vol. 34, No. 3, pp. 266 - 267, 1998
- [46] R.A. Soref, D.L. McDaniel Jr. and B. Bennett, "Guided-wave intensity modulators using amplitude-and-phase perturbations," *Lightw. Technol. J.*, Vol. 6, No. 3, pp. 437 - 444, 1988

- [47] P. Maat, “InP-Based integrated MZI switches for optical communication,” Ph.D. dissertation, Delft University of Technology, 2001
- [48] H.Y. Wong, “InGaAs/InAlGaAs monolithically integrated Mach-Zehnder interferometer devices,” Ph.D. dissertation, Department of Electronics and Electrical Engineering, University of Glasgow, 2005
- [49] Y. Ueda, S. Nakamura, Utaka, Katsuyuki and T. Shiota, “Very-low-current operation of InAlGaAs/InAlAs/InP Mach-Zehnder interferometer-type multi-mode interference photonic switch (MIPS-MZ)”, Int’l conference on Indium Phosphide and Related Materials, IEEE, pp. 1 – 3, 2008
- [50] P. Jain, D. Tanaka and H. Tsuda, “Mach Zehnder Interferometer Optical Switch Using Phase-Change Material”, Int’l conference on Photonics in Switching (PS), 2012
- [51] Sh. Cao, L. Sun, and M. Savoie, “2×2 MMI-MZI GaAs-GaAlAs Carrier-Injection Optical Switch”, IEEE photonics society summer topical meeting series, 2010
- [52] R. R. Palupi, A. Syahriar¹, A. H. Lubis, S. Rahardjo and Sardjono, “Simulation of Mach Zehnder Interleaver Based Thermo-Optic Effect in L-Band Range”, IEEE regional symposium on micro and nanoelectronics (RSM), pp. 269 – 272, 2013
- [53] H.Y. Wong, W.K. Member and W.K. Tan, “Current injection tunable monolithically integrated InGaAs–InAlGaAs asymmetric Mach–Zehnder interferometer using quantum-well intermixing”, *Photon. Technol. Lett.*, IEEE, Vol. 17, No. 8, pp. 1677 – 1679, 2005
- [54] F. Wang, Jianyi Yang, L. Chen, X. Jiang, and M. Wang, “Optical Switch Based on Multimode Interference Coupler”, *IEEE photonics technology letters*, Vol. 18, No. 2, pp. 421 – 423, 2006
- [55] Y. Ma, S. Park, L. Wang and S.T. Ho, “Ultracompact multimode interference 3-dB coupler with strong lateral confinement by deep dry etching”, *Photon. Technol. Lett.*, IEEE, Vol. 12, No. 5, pp. 492 – 494, 2000

- [56] J. Zhou and P. Gallion, "Operation Principles for Optical Switches Based on Two Multimode Interference Couplers", *J. Lightwave Technol.*, Vol. 30, No. 1, pp. 15 – 21, 2012
- [57] M. Tajaldini, M. Z. M. Jafri, "All Optical Switch Using Ultra compact Multi Mode Interference Coupler", *IEEE int'l conference on semiconductor electronics (ICSE)*, pp. 370-373, 1988
- [58] M. Kolesik, M. Matus and J.V. Moloney, "All-optical Mach-Zehnder-interferometer-based demultiplexer-a computer simulation study", *Photon. Technol. Lett., IEEE*, Vol. 15, No. 1, pp. 78-80, 2003
- [59] A. Tervonen, P. Poyhonen, S. Honkanen, and M. Tahkokorpi, "A guided-wave Mach-Zehnder interferometer structure for wavelength multiplexing", *IEEE Photon. Technol. Lett.*, Vol. 3, No. 6, 1991
- [60] H. Wei, J. Yu, Z. Liu and X. Zhang, "Signal bandwidth of general $n \times n$ multimode interference couplers", *Lightw. Technol. J.*, Vol. 19, No. 5, pp. 739 – 745, 2001
- [61] R. Hanfoug, L.M. Augustin, Y. Barbarin, J.J.G.M. van der Tol, "Reduced reflections from multimode interference couplers", *Electron. Lett.*, Vol. 42, No. 8, pp. 465 – 466, 2006
- [62] D. Dai, and S. He, "Optimization of ultracompact polarization-insensitive multimode interference couplers based on Si nanowire waveguides", *Photon. Technol. Lett., IEEE*, Vol. 18, No. 19, pp. 2017 – 2019, 2006
- [63] P.P. Sahu, "A tapered structure for compact multimode interference coupler", *IEEE Photon. Technol. Lett.*, Vol. 20, No. 8, pp. 638 – 640, 2008
- [64] M.A. Swillam, M.H. Bakr and X. Li, "Efficient design of integrated wideband polarization splitter/combiner", *J. Lightw. Technol.*, Vol. 28, No. 8, pp. 1176 – 1183, 2010
- [65] D.J. Thomson, Y. Hu, G.T. Reed and J.M. Fedeli, "Low loss MMI couplers for high performance MZI modulators", *IEEE Photon. Technol. Lett.*, Vol. 22, No. 20, pp. 1485 – 1487, 2010

[66]K.S. Chiang and Q. Liu, “Formulae for the design of polarization-insensitive multimode interference couplers”, IEEE Photon. Technol. Lett., Vol. 23, No. 18, pp. 1277 – 1279, 2011